

This is an Open Access document downloaded from ORCA, Cardiff University's institutional repository:<https://orca.cardiff.ac.uk/id/eprint/114244/>

This is the author's version of a work that was submitted to / accepted for publication.

Citation for final published version:

Long, Katherine R., Newland, Ben , Florio, Marta, Kalebic, Nereo, Langen, Barbara, Kolterer, Anna, Wimberger, Pauline and Huttner, Wieland B. 2018. Extracellular matrix components HAPLN1, lumican, and collagen I cause hyaluronic acid-dependent folding of the developing human Neocortex. *Neuron* 99 (4) , 702-719.e6. 10.1016/j.neuron.2018.07.013

Publishers page: <http://dx.doi.org/10.1016/j.neuron.2018.07.013>

Please note:

Changes made as a result of publishing processes such as copy-editing, formatting and page numbers may not be reflected in this version. For the definitive version of this publication, please refer to the published source. You are advised to consult the publisher's version if you wish to cite this paper.

This version is being made available in accordance with publisher policies. See <http://orca.cf.ac.uk/policies.html> for usage policies. Copyright and moral rights for publications made available in ORCA are retained by the copyright holders.



Extracellular matrix components HAPLN1, lumican and collagen I cause hyaluronic acid-dependent folding of the developing human neocortex

Katherine R. Long¹, Ben Newland^{2†}, Marta Florio^{1#}, Nereo Kalebic¹, Barbara Langen¹, Anna Kolterer³, Pauline Wimberger³ and Wieland B. Huttner^{1*}

¹Max Planck Institute of Molecular Cell Biology and Genetics, Pfotenhauerstraße 108, D-01307 Dresden, Germany.

²Leibniz Institute of Polymer Research Dresden (IPF), Hohe Straße 6, 01069 Dresden, Germany

³Technische Universität Dresden, Universitätsklinikum Carl Gustav Carus, Klinik und Poliklinik für Frauenheilkunde und Geburtshilfe, Fetscherstraße 74, D-01307 Dresden, Germany

[†]Sir Henry Wellcome Postdoctoral Fellow of the Brain Repair Group, School of Biosciences, Cardiff University, Cardiff, CF10 3AX, Wales, UK

[#]Present Address: Department of Genetics, Harvard Medical School, Boston, MA 02115, USA

*Lead Contact. Correspondence to: huttner@mpi-cbg.de

Summary: Neocortical expansion, thought to underlie the cognitive traits unique to humans, is accompanied by cortical folding. This folding starts around gestational week (GW) 20, but what causes it remains largely unknown. Extracellular matrix (ECM) has been previously implicated in neocortical expansion and here we investigate the potential role of ECM in the formation of neocortical folds. We focus on three specific ECM components localized in the human fetal cortical plate (CP): hyaluronan and proteoglycan link protein 1 (HAPLN1), lumican and collagen I (collectively, HLC). Addition of HLC to cultures of human fetal neocortex (11-22 GW) caused local changes in tissue stiffness, induced CP folding, increased CP hyaluronic acid (HA) and required the HA-receptor CD168 and downstream ERK signaling. Importantly, loss of HA reduced HLC-induced and 22 GW physiological nascent

folds. This was altered in samples with neurodevelopmental disorders, indicating it may be a useful system to study such disorders.

Key words: Human neocortex, neocortex folding, ECM, HAPLN1, lumican, collagen, hyaluronic acid, neocortex development, neurodevelopmental disorders.

Introduction

The evolutionary expansion of the neocortex is thought to be a prerequisite for the higher cognitive functions that are unique to humans. A key aspect of this expansion is the formation of cortical folds, called gyri and sulci, that allow enlargement of the cortical surface area within the confinement of the skull (Dehay et al., 2015; Fernandez et al., 2016; Florio and Huttner, 2014; Lewitus et al., 2013; Lui et al., 2011; Rakic, 2009; Sun and Hevner, 2014; Zilles et al., 2013). Regulation of the number and position of folds is fundamental to proper brain function. Both a decrease in folding (e.g. disorders such as lissencephaly) as well as an increase in folding (e.g. aberrantly small folds as observed in polymicrogyria) are often associated with cognitive defects (Bae et al., 2015; Barkovich et al., 2012; Lian and Sheen, 2015; Parrini et al., 2016; Reiner, 1999; Sun and Hevner, 2014).

Despite recent advances in the field that have reported molecular manipulations capable of promoting cortical folding (Bae et al., 2014; Borrell, 2018; Florio et al., 2015; Li et al., 2016; Masuda et al., 2015; Matsumoto et al., 2017; Shinmyo et al., 2017; Stahl et al., 2013) and have modelled mechanical aspects of folding (Bayly et al., 2014; Mota and Herculano-Houzel, 2015; Tallinen et al., 2016), how defined molecules generate cortical folds in mechanistic terms remains largely unknown. Recent studies examining gene expression in the developing neocortex (Fietz et al., 2012; Florio et al., 2015; Miller et al., 2014; Nowakowski et al., 2017; Pollen et al., 2015; Pollen et al., 2014) identified evolutionary changes in gene expression patterns between the embryonic neocortex of mouse, which remains smooth (lissencephalic), and the fetal neocortex of human, which folds during development (gyrencephalic). Notably, these studies highlighted an increase in the expression of extracellular matrix (ECM) components in human germinal zones and cortical progenitor cells compared to mouse (Fietz et al., 2012; Florio et al., 2015). This is especially true for the outer subventricular zone (OSVZ) (Fietz et al., 2012), the germinal zone of the human neocortex that generates the increased numbers of neurons underlying neocortical expansion (Dehay et al., 2015; Smart et al., 2002). It has been previously shown that ECM receptors can regulate the proliferation of cortical progenitors cells (Fietz et al., 2010; Stenzel et al., 2014). Together, these data raise the possibility that ECM may have a role in the expansion of the human neocortex. Here we investigate the function of specific ECM components, found to be more highly expressed in the human neocortex within these datasets, in human neocortex development.

Results

Selection of HAPLN1, lumican and collagen I

We searched the existing datasets (Albert et al., 2017; Fietz et al., 2012; Florio et al., 2015) for specific ECM components (from the core matrisome (Naba et al., 2012)) that are more highly expressed in the human than mouse germinal zones and cortical progenitor cell populations. To identify ECM components associated with neocortex expansion, we selected genes that were expressed by neural progenitor cells (NPCs) in human but not in mouse (see Methods for search strategy; Fig 1A). In particular, from these genes more highly expressed in human NPCs, we selected those whose expression was down regulated during mouse neurogenesis, i.e. that were expressed early in mouse development, during the expansion of neuroepithelial cells (E9.5 (Albert et al., 2017)), but were no longer expressed during the peak of neurogenesis (E14.5 NPCs (Florio et al., 2015)). This search led to the identification of three candidate ECM components: hyaluronan and proteoglycan link protein 1 (HAPLN1), the proteoglycan lumican, and the collagen I subunit alpha 2 (see Figure S1A, B for mRNA levels (Fietz et al., 2012; Florio et al., 2015), Table 1).

To confirm that these ECM components were expressed at the protein level, immunofluorescence (IF) of HAPLN1, lumican and collagen I was performed on 13 GW human neocortex and E14.5 mouse neocortex. In the mouse, HAPLN1 and collagen I were absent from the neocortex, as expected, but lumican was detected throughout the neocortical wall (Figure 1B). Interestingly, in the human tissue, lumican was also found throughout the neocortical wall, whereas HAPLN1 and collagen I were more concentrated in the CP than in any other region (Figure 1B, S1C), despite the mRNAs for these three ECM components being predominantly found in the germinal zones (rather than CP) of human fetal neocortex (Fietz et al., 2012) (Figure S1A). Our observations that HLC are more highly concentrated in the CP therefore suggest that these ECM components can travel far from their site of origin and that progenitor cells may play a role in determining the ECM composition of the developing human CP.

HAPLN1, lumican and collagen I induce folding of the CP of 11-14 GW human neocortex.

ECM components often interact in a network and their function may therefore be greatly affected by their environment. As the ECM composition differs between the mouse and human (Fietz et al., 2012; Florio et al., 2015), we used two different human fetal neocortex explant systems to study the function of HAPLN1, lumican and collagen I in human neocortex development and expansion. First, we added recombinant human HAPLN1 and lumican (each at 5 $\mu\text{g/ml}$) to collagen I-embedded organotypic slice cultures of 11-14 GW human neocortex. Compared to control (collagen I-embedding only), HAPLN1 and lumican addition had a striking effect, inducing folding of the CP after just 24 hours (h) of treatment (Figure 2A, S2A). Quantification of this, by adopting the method used to measure the gyrencephaly index (GI) in vivo (Zilles et al., 1988), revealed that HAPLN1 and lumican addition increased GI from 1.0 (control) to 1.8 (Figure 1B). HAPLN1 appeared to be the primary component required, as its addition alone increased GI to 1.5 (Figure 2A, C), whereas that of lumican alone did not significantly increase GI (Figure 2C).

In order to characterize the ECM-induced folds, we performed IF for nestin, an intermediate filament marker of radial glia progenitors (Dahlstrand, 1995). This revealed three key morphological features of the radial glia basal processes; they continued to reach the pial surface, followed the curvature of the folds and displayed a fanned appearance (Figure S2A). These features are hallmarks of physiological folds, such as those observed in the ferret (Reillo et al., 2011). We also performed IF for laminin, which showed that the basal lamina invaginated with the folds (Figure 2D), similar to physiological folds observed at later developmental stages.

To corroborate these findings in a different explant system, we next examined the effects of HAPLN1, lumican and collagen I in free-floating human fetal neocortex tissue culture (FFTC). This consists of dissected human fetal neocortex tissue freely floating in medium, either without (control) or with the addition of the three ECM components (from now on referred to as HLC-treatment). HLC-treatment of FFTCs of 11-14 GW human neocortex induced folding of the CP in 24 h (Figure 2B, G), increasing GI to ~ 1.5 (Figure 2F). The lesser increase in GI in comparison to the organotypic slice cultures may reflect the reduced penetration of HLC throughout the tissue, due to its greater thickness. However, the recombinant proteins used were still able to penetrate the neocortical tissue in this floating culture system, as shown by detection of the His-tags of recombinant HAPLN1 and lumican throughout the neocortical wall (Fig S1E, F).

As observed in organotypic slice cultures, the laminin-stained basal lamina invaginated with the folds (Figure 2E), and the nestin-stained radial glia processes reached the pial surface and followed the fold curvature, displaying a fanned appearance (Figure 2G). Together these data indicate the ECM components HLC can induce folds in 11-14 GW human neocortex explants that share key morphological features with folds observed at later developmental stages.

HLC-induced folds form in under 24 h

We next performed time-lapse imaging of organotypic slice cultures of 12 GW human neocortex stained with a vital nuclear dye to observe the formation of the folds over time. Control slices (no ECM addition) showed no observable change in CP morphology during 24 h of culture (Figure 2I top, movie S1), whereas addition of HLC led to the formation of folds specifically at the basal (pial) side of the slices between 16 and 24 h (Figure 2I bottom, movie S2).

Consistent with the timing observed from the time-lapse imaging, the GI of 12-15 GW human neocortex in FFTC was unaltered after 8 h (remaining at ~1.0), slightly increased by 16 h and significantly increased by 24 h (Figure S2B) upon HLC-treatment. HLC-treatment did not cause a further GI increase after 48 and 72 h of culture as compared to 24 h (Figure S2C-E).

Folding does not occur with other ECM combinations

To examine if the specific combination of HLC was required for folding, we tested different ECM components and combinations. Collagen I, though insufficient alone (Figure 2C, S2F), was required for folding, as addition of only HAPLN1 and lumican did not significantly increase GI (Figure 2H). This permissive action was specific to collagen I, as addition of HAPLN1, lumican and collagen IV did not induce folding of 14-18 GW human neocortex in FFTC (Figure S2G, H). All three HLC components were required for the greatest increase GI in FFTC, as neither the individual HLC components alone nor collagen I plus HAPLN1 (without lumican) were able to increase GI to the level obtained by HLC-treatment in this system (Fig S2F).

In contrast to the addition of HAPLN1 and lumican, addition of laminin-211 and collagen IV to collagen I-embedded slice cultures did not induce folding of 11-14 GW human neocortex

(Figure S2I). Lack of folding of 12-15 GW human neocortex was also observed upon addition of a commonly used basement membrane-derived ECM extract to FFTCs (Figure S2J). This indicates that it is a specific combination of ECM components, rather than any increase in ECM, that can induce such folding of the human CP.

HLC does not induce folding in mouse or ferret neocortex

In order to investigate if this effect of HLC was conserved across different species, we next examined if HLC could induce folding in developing mouse (lissencephalic) and ferret neocortex (gyrencephalic, GI 1.7 vs. human GI 2.6, (Lewitus et al., 2014)) (Figure S3). Several stages were investigated; embryonic day (E) 14.5 mouse and E33 ferret (equivalent to 11-14 GW human) neocortex in organotypic slice culture, and E33, postnatal day (P) 9 and P15 ferret (physiological folding stages) neocortex in FFTC. Remarkably, addition of HLC did not induce folding nor an increase in GI in mouse or ferret neocortex slice cultures after 24 h (Figure S3A-D), or in ferret FFTCs after 2, 3 or 4 days (Figure S3E-L). As one might have expected the ferret as a gyrencephalic animal to be responsive to HLC-treatment, these data suggest that the role of HLC in neocortical folding may not be conserved in ferret, or that aspects of the pathway required to induce such folding are absent in these species.

IF for HLC reveals differences between ferret and human

Indeed, IF for HAPLN1, lumican and collagen I in the developing ferret neocortex revealed differences between ferret and human. Lumican showed a broad distribution across the developing neocortical wall in both species (Figure 1B, S4A-C). However, HAPLN1 and collagen I were both absent in E33 ferret neocortex (Figure S4A), but were observed at a low, relatively uniform level throughout the cortical wall at P9 and P15 (during fold formation, Figure S4B, C).

In comparison, IF for HAPLN1, lumican and collagen I in the human neocortex revealed that all three ECM components were detected in the CP at 13 GW (Figure 1B), 18 GW (just prior to the onset of folding, Figure 3A), 22 GW (just after the onset of folding, Figure 3B) and at 38 GW (when folding is relatively established, Figure 3C). HAPLN1 and lumican were also detected throughout the neocortical wall at 18 GW, unlike collagen I (Figure 3A). At the later stages (22 and 38 GW) all three components were detected in both the developing gyrus and sulcus (Figure 3B, C). At 38 GW, the staining for HAPLN1 has become more diffuse, as seen in adult cortex (Uhlen et al., 2015) and lumican and collagen I have become more fibrous.

Together, these data suggest that HLC are present in the CP of the human developing neocortex both before and during fold formation and the expression of these ECM components differs between human and ferret.

HLC-induced folding requires hyaluronic acid

We next sought to obtain insight into the cellular and molecular mechanisms underlying the HLC-induced folding of human fetal neocortex. We first considered increased proliferation that would lead to increased neuron production. However, analysis of various markers of cycling and mitotic cells showed no significant increase in proliferation (Figure S5). Additionally, the use of an inhibitor of cell proliferation (mitomycin C (Hung et al., 1996)) alongside HLC-treatment in 11-14 GW human neocortex FFTCs did not significantly reduce the GI, indicating that HLC-induced folding does not require progenitor proliferation (Figure S5).

Second, comparative transcriptome analysis of 12-14 GW human neocortex after 16 h of control and HLC-treatment in FFTC (when HLC-induced folding has just started) revealed only minor changes in gene expression, which by gene ontology analysis were found to be mostly related to ECM and cell adhesion (Figure S6, Table S1). This suggests that HLC-induced folding does not involve major changes in gene expression, but only a low level of differential gene expression that primarily concerns ECM and cell adhesion.

Finally, we analyzed the level and localization of hyaluronic acid (HA), as HAPLN1 is known to interact with and modulate this key ECM component (Binette et al., 1994). Immunostaining revealed an increase in the relative level of HA in the CP after 24 h of HLC-treatment of 11-14 GW human neocortex FFTCs (Figure 4A-B). This increase was already observed after 8 and 16 h of HLC-treatment (Figure 4C), suggesting that an increase in HA levels in the CP precedes the appearance of HLC-induced folds. This early increase in HA is reflected by an increase in the expression of the enzymes that synthesize it, HAS1-3, 6 h after HLC-treatment (Fig S6E), along with a reduction in the expression of the enzymes that degrade it, HYAL2 and 3 (Fig S6E). These changes in gene expression appeared to be transient, as they were no longer detected after 8 h of HLC-treatment (Fig S6E). Interestingly, HA was seen to be present throughout the CP at stages of physiological folding in the human neocortex, 22 GW and 38 GW (Figure 3C, D), showing a similar diffuse staining pattern as HAPLN1 at 38 GW (Figure 3D).

In contrast to the human, HLC-treatment of E33 ferret neocortex in FFTC did not significantly increase the level of HA in the CP (Figure S3M, N). Moreover, addition of HA alongside HLC-treatment did not induce folding of E33 ferret neocortex in FFTC (Figure S3O), suggesting that it is not the lack of HA that renders the ferret neocortex non-responsive to HLC-treatment.

To determine if HA is required for HLC-induced folding of human fetal neocortex, we added a mixture of hyaluronidases (hyals), which degrade HA, together with HLC to 12-14 GW human neocortex in FFTC. Addition of hyals to HLC-treatment reduced the level of HA in the CP to that of control (Figure 4B, D) and prevented the HLC-induced cortical folding, maintaining the GI near 1.0 (Figure 4D, E). Strikingly, hyals were able to reduce HLC-induced folding when added after 24 h of HLC-treatment, returning the GI back to near 1.0 (Figure 4E, movie S3) and reducing the level of HA (Fig S7A). Addition of 4-methylumbelliferone, an inhibitor of HA synthases (HAS) (Rilla et al., 2004), was also able to block the HLC-induced cortical folding, suggesting synthesis of HA was required for folding to occur (Figure 4F). In contrast to the effect of hyals, addition of chondroitinase ABC (chondABC), which targets a glycosaminoglycan component of the ECM distinct from HA, did not prevent HLC-induced folding (Figure 4E) or reduce the level of HA (Fig S7A, B). Together, these observations indicate that HA exerts a key role in HLC-induced folding of early human neocortex.

HLC induces folding in 22 GW human neocortex in FFTC.

As HLC and HA are expressed in the CP at later stages of human neocortex development (Figure 3C, D), this prompted us to investigate whether the HA-dependent HLC-induced folding described so far with 11-15 GW human neocortex is of relevance for physiological folding, which is known to begin at a later stage of human fetal neocortical development (~20 GW) (Zilles et al., 2013). To do this we used 22 GW human neocortex in the FFTC system, as nascent folds are already present in the CP at this developmental stage, as indicated by an increased GI (referred to as inherent GI) of 1.15 in both 22 GW human neocortex not subjected to FFTC (Figure 4H) and subjected to control treatment in FFTC (Figure 4G-K). We next subjected 22 GW human neocortex in FFTC to HLC-treatment for 4 days and found that this significantly increased GI above the inherent value (from 1.15 to ~1.3; Figure 4G, I, J). At this developmental stage, no GI increase by HLC was observed after only 24 h of

treatment (Figure S7D). This could be due to increased thickness of the 22 GW tissue and CP, as more time would be needed for HLC to penetrate the CP and initiate folding.

The thickness of the CP could also help to explain why the HLC-induced folds observed at 22 GW were larger than those observed at earlier stages. The thickness of the CP has been previously hypothesized to influence the number and size of cortical folds (Bayly et al., 2014; Richman et al., 1975), where the intergyral distance is thought to be related to the thickness of the cortical plate. In line with this theory, the folds present in the 11-16 GW tissue have a relatively smaller intergyral distance than the inherent physiological folds observed in the 22 GW tissue (Figure S7E), whereas the folds in 22 GW tissue treated with HLC are more similar to the inherent folds present at 22 GW (Figure S7E). These data suggest that HLC-treatment induces a level of folding that is related to the thickness of the CP, resulting in a smaller intergyral distance in 11-16 GW samples than 22 GW samples.

Loss of HA reduces the inherent folding present in 22 GW human neocortex in FFTC

As addition of HLC was able to increase the level of folding in 22 GW neocortex, we next examined if this required HA, as in the earlier stages of neocortex examined. As HA is known to generally turn over relatively quickly (Fraser et al., 1997), we used a HAS inhibitor (Figure S7C, F) and hyals to remove HA in this later stage tissue. This combination blocked the HLC-induced increase in GI observed after 4 days of FFTC (Figure 4G) but, more strikingly, also reduced the inherent GI to ~1.0 (Figure 4G, H). This reduction of inherent GI to ~1.0 was also observed when either the HAS inhibitor, hyals or a combination of both were added to 22 GW neocortex in FFTC for 4 days (without HLC) (Figure 4H, I K) or for 24 h (Figure S7G). Overall, these data suggest that HA is important to maintain the nascent physiological folds present in 22 GW neocortex.

This was not the case for the early stages of folding in the ferret neocortex. Treatment of P15 ferret neocortex with hyals and HAS inhibitor for 2 days in FFTC did not reduce its inherent GI (1.2-1.3, Figure S3P, Q) as we observed in the human neocortex. This is consistent with the inability of HLC-treatment to raise HA levels in the CP (Figure S3M, N), or of HA supplementation to HLC-treatment to increase GI of E33 ferret neocortex (Figure S3O).

HLC-induced folding replicates aspects of physiological nascent folds at 22 GW

Our data indicate that HLC-induced folding and physiological nascent folds both required HA in the CP, suggesting a shared feature between the two mechanisms. To examine if there were other similarities between HLC-induced and nascent physiological folds, we next investigated the degree of folding in the CP layers. Physiological folding initially occurs more so in the upper most CP layers, with the deeper layers becoming more folded over the course of development. In keeping with this, the nascent physiological folds present at 22 GW show increased folding the upper neuronal layers in comparison to the deeper layers, as observed by IF for TBR1 and CTIP2, two markers of deep-layer neurons with distinct expression patterns in layers VI and V respectively (Molyneaux et al., 2007) (Figure 5A). HLC-induced folding of 15 GW human neocortex replicated this, as the CTIP2 positive neuronal layer was more folded than the TBR1 layer below it (Figure 5B), closely resembling the nascent physiological folds present at 22 GW.

During the formation of these nascent folds and rearrangement of neuronal layers, the CP undergoes large morphological changes that could lead to differential spacing of cells within the developing gyrus versus the sulcus. Indeed, when we examined the nuclei within the nascent gyrus of non-cultured 22 GW neocortex, we observed a greater distance between them than in comparison to the developing sulcus (Figure S7H, I). This aspect of physiological nascent folds was also observed in the HLC-induced folds of 11-14 GW neocortex in FFTC (Figure 5C-E). This increase in nuclei distance could already be observed at 8 h (slight shift right in frequency distribution, Figure S7J, K) and was overt by 16 h (Figure S7L, M), indicating that the distance between nuclei increased as HLC-induced folding proceeded. Taken together, these data indicate that HLC-induced folds replicate specific aspects of the physiological nascent folds observed at 22 GW.

HLC induce a specific pattern of ECM stiffness that is present in physiological nascent folds

To further investigate the mechanism underlying HLC-induced folding, we next examined ECM stiffness within the CP. There were two reasons for this, first that ECM stiffness has been linked to changes in cell migration and spacing (Miron-Mendoza et al., 2010), and second that the HLC components have been previously shown to modify ECM organization (Binette et al., 1994; Schaefer and Iozzo, 2008). Changes in ECM organization, such as the increase in HA in the CP after HLC-induced folding (Figure 4A, B), can lead to changes in ECM stiffness, suggesting that this may be altered in HLC-induced folding.

To explore this, we performed atomic force microscopy (AFM) with 12-14 GW human neocortex tissue that following FFTC had undergone freeze-thawing (Figure S8A, B), an established approach to examine the ECM within various tissues irrespective of cell viability (Graham et al., 2010). AFM revealed that the CP gyri formed upon HLC-treatment were stiffer than the neighboring sulci, the stiffness of which was comparable to control CP (Figure 5F-H). This pattern of alterations in ECM stiffness was already detectable after 8 h of HLC-treatment, prior to fold formation (Figure S8C). It was then overt after 16 h of HLC-treatment, when HLC-induced folding has just started (Figure 5G, S8D). Importantly, increased ECM stiffness in nascent gyri compared to sulci in non-cultured 22 GW neocortex was also observed by AFM (Figure 5I), suggesting that this is a physiological characteristic of nascent folds.

The observed increase in ECM stiffness in nascent gyri compared to sulci (Figure 5I) and the HA-dependence of the inherent GI (Figure 4H, I, K) of 22 GW human neocortex raised the possibility of a causal relationship between HA levels and the ability of the ECM to undergo alterations in stiffness. Indeed, treatment of 22 GW human neocortex in FFTC for 4 days with hyals and HAS inhibitor reduced the range of stiffness values to half of control, as determined by AFM (Figure 5J). Furthermore, in line with the notion that increases in ECM stiffness underlie the formation of gyri vs. sulci upon HLC-treatment, as observed with 12-14 GW human neocortex (Figure 5F-H, Figure S8C, D), HLC-treatment of 22 GW human neocortex in FFTC for 4 days dramatically increased the range of stiffness values compared to control (Figure 5J).

Interestingly, although HLC-treatment of E33 ferret neocortex in FFTC was unable to induce folding in the developing ferret neocortex, we did observe that HLC-treatment was able to cause local increases in ECM stiffness in the CP (Figure S3R, S). This suggests that HLC can induce some changes in the ferret neocortex, but that it cannot induce folding. This may be due to a lack of other downstream components in the ferret neocortex, or that these components are not activated by such changes in ECM stiffness.

HA receptor CD168 and downstream ERK signaling are required for HLC-induced folding

We next further investigated the mechanism behind the HA-dependent, HLC-induced folds in the human CP. To obtain mechanistic insight into the HA-dependency we examined the expression of the two major HA-receptors, CD44 and CD168 (also called *Receptor for HA-Mediated Motility (RHAMM)*) (Casini et al., 2010; Dzwonek and Wilczynski, 2015; Lynn et al., 2001; Nagy et al., 1995). IF of 13 and 22 GW human neocortex showed that CD44 was uniformly distributed in the CP at both developmental stages (Figure 6A, B). However, although CD168 was distributed throughout the CP at 13 GW (Figure 6A), it was more highly expressed in nascent gyri than sulci at 22 GW (Figure 6B).

These data raised the possibility that activation of CD168 or CD44 may be required for HLC-induced folding of the human CP. We therefore performed HLC-treatment of 12-15 GW human neocortex in FFTC in the presence of a CD168 antibody and a CD44 antibody. The CD168 antibody essentially blocked the HLC-induced folding, maintaining the GI at 1.0 (Figure 6C, D), whereas the CD44 antibody did not significantly reduce the HLC-induced GI increase (Figure 6C, D). Interestingly, the CD168 antibody also blocked the increase in HA in the CP observed after HLC-treatment, unlike the CD44 antibody (Figure 6E). This indicates that the HA-receptor CD168, rather than CD44, is required for the HA-dependent, HLC-induced folding of the human CP.

CD168 and CD44 have been shown to regulate neuron migration via the ERK pathway (Lynn et al., 2001; Zhang et al., 1998). We therefore next performed IF for phospho-ERK (pERK), a marker of active ERK signaling, on 12-15 GW human neocortex in FFTC. We observed that HLC-treatment activated ERK signaling, increasing the pERK level to 1.5 times that of control (Figure 6F). This increase was already observed after 8 h of HLC-treatment (Figure 6G), suggesting it precedes the appearance of HLC-induced cortical folding, and was equally increased in gyri compared to their neighboring sulci after 24 h of HLC-treatment (Fig 6H). This activation of ERK by HLC-treatment was not significantly lowered by the CD44 antibody (Figure 6F), but was significantly reduced by the CD168 antibody, which reduced pERK levels below that of control (Figure 6F). Of note, the degradation of hyaluronic acid by addition of hyals prevented the HLC-induced increase in pERK levels, maintaining them at the level of the control (Fig 6I).

This indicated that ERK activation by HLC-treatment is downstream of the HA receptor CD168. To examine if ERK signaling was required for HLC-induced folding, we next added

an inhibitor of ERK1/2 in addition of HLC-treatment. This ERK1/2 inhibitor, which reduced the levels of the ERK downstream target p90RSK in the CP (Fig S7N, O), blocked the HLC-induced increase in GI in 12-16 GW human neocortex in FFTC (Figure 6J, K), maintaining the GI at 1.0. Together, these data suggest that HLC-induced folding of the human CP requires the activation of ERK signaling downstream of the HA-receptor CD168.

ECM stiffness requires HA and is upstream of CD168/ERK signaling

As HLC-induced folds increased ECM stiffness and require CD168/ERK signaling, we next investigated the connection between these two features. To do so, we used AFM to examine how ECM stiffness was affected by the addition of the CD168 antibody, ERK inhibitor, chondABC or hyals to HLC-treatment in 13-15 GW human neocortex in FFTC for 24 h. The addition of either the CD168 antibody or ERK inhibitor was sufficient to block the HLC-induced increase in GI (Fig 6D, J), but did not reduce the increased ECM stiffness values measured by AFM after HLC-treatment (Fig S8E). In contrast, the addition of hyals was sufficient to block both the HLC-induced increase in GI (Fig 4E) and the increased ECM stiffness (Fig S8E). This reduction in ECM stiffness was not due to a general disruption of the ECM, as addition of chondABC, which did not block the HLC-induced increase in GI, did not reduce the HLC-induced increase in ECM stiffness either (Fig S8E). This indicates that HA is required for the HLC-induced increase in ECM stiffness, and that this HA-linked increased stiffness is upstream of CD168/ERK signaling. Taken together, these data suggest that both the HA-linked ECM stiffness and the downstream CD168/ERK signaling are required for HLC-induced folding.

HLC-induced folding as an assay to examine neurodevelopmental disorders (NDDs)

Our observations that HLC-treatment increased the GI not only of 11-14 GW (Figure 2) but also of 22 GW (Figure 4G, I, J) human neocortex in an HA-dependent manner, and was able to replicate aspects of physiological nascent folds, suggest that this system may be a useful model to study aspects of physiological folding in the human CP. In particular, HLC-induced folding could have potential as an assay in which to study various human NDDs. We therefore examined human neocortex samples from fetuses with altered neocortex development, notably five cases of Down syndrome (DS) (trisomy 21). Remarkably, in contrast to 11-15 GW non-trisomy human neocortex (Figure 2), HLC-treatment of 14-17 GW DS neocortex in FFTC did not induce folding (Figure 7A-C). However, when a later developmental stage of DS (21 GW) was examined, HLC-treatment was able to significantly

increase GI above the inherent value (from ~1.1 to ~1.2) of this neocortex tissue in a HA-dependent manner (Figure 7F, G), as was the case for 22 GW non-trisomy human neocortex (Figure 4G, I, J).

Analysis of two other fetal samples with altered neocortex development, prenatal methamphetamine exposure (PME) (12 GW) and 2p16.3 microdeletion (16 GW) was also performed. These two developmental disorders are interesting as PME has been previously reported to affect cortical folding in animal models (Jablonski et al., 2016), whereas in contrast, 2p16.3 microdeletions are not known to affect these aspects of cortical development, but rather affect synaptic activity and susceptibility to psychiatric disorders (Vinas-Jornet et al., 2014). Accordingly, HLC-treatment in FFTC did not induce folding in the PME sample, but was able to significantly increase the GI in the 2p16.3 microdeletion sample (Figure 7B, D, E).

Consistent with these data, the relative level of HA in the CP was only increased in the 2p16.3 microdeletion sample (small increase) and the 21 GW DS sample (three-fold increase) after HLC-treatment when compared to control, whereas no relative increase in HA was observed in the PME sample or the 14 GW Downs sample (Figure 7H, I). Taken together, these data suggest HLC-induced folding revealed known aspects of various NDDs including abnormal folding after PME and normal folding in a 2p16.3 microdeletion sample. It also revealed aspects of disorders that are not yet fully understood, such as the delayed response of DS tissue to HLC-induced folding which may reflect the developmental delay or slight reduction in sulcal depth seen in some DS cases (Annus et al., 2017). Together, these data suggest that HLC-induced folding has potential as an assay in which to further study such NDDs.

Discussion

In conclusion, our study presents three major findings. Firstly, we have established an *in vitro* model of fetal human neocortical folding that can be used for the mechanistic dissection of fold formation and to investigate the NDDs associated with abnormal neocortical folding. Secondly, we have established a key role of the specific ECM components HAPLN1, lumican and collagen I in the formation of cortical folds in the fetal human neocortex. Thirdly, we have established that local changes in tissue stiffness, rearrangement of HA and

the HA receptor CD168 play key roles in the regulation of early folding in the human neocortex.

There are currently several concepts as to how neocortical folds are formed, ranging from mechanical to genetic (Borrell, 2018; Kroenke and Bayly, 2018). Genetic studies have identified areas in the developing ferret neocortex that are predetermined to fold (De Juan Romero et al., 2015) and have shown that individual genes can induce folding in mice (Florio et al., 2015; Stahl et al., 2013). Of note from the mechanical models, it has been proposed that folding occurs due to the non-uniform tangential basal expansion observed in neocortical development (Tallinen et al., 2014; Tallinen et al., 2016). Folding of the human neocortex is most likely regulated by a combination of these genetic and mechanical factors, which will interact and modulate each other. Here, our data suggest the ECM as an interesting candidate to link these two models, as manipulation of the ECM can induce and alter the initial stages of folding, in part by modifying ECM stiffness. This suggests that transcriptional regulation of ECM expression, and the factors that modulate it, could be important for the regulation of physiological folding in human neocortex development.

Although HLC-induced folding replicated specific aspects of physiological nascent folds, several aspects are clearly different. For example, HLC-induced folding did not require the proliferation of progenitors to induce folding and it occurred prematurely, in fetal tissue obtained weeks prior to when folding starts *in vivo* (~20 GW) and at a much faster rate. Normally folding occurs over the course of weeks, not within a few hours as with HLC-induced folding, allowing increased neuron production over time to play a key role in fold formation. In support of this, genes differentially expressed in areas predetermined to form gyri versus sulci are known to increase neuron production (De Juan Romero et al., 2015). However, when 22 GW human fetal neocortex was treated with HLC, folds did not form in 24 h, but instead in 4 days. This would be more in-keeping with the physiological timeline of cortical folding and suggests that the younger tissue folds faster due to its smaller size, i.e. a thinner CP. In physiological development, the endogenous HLC and HA present in the 20 GW human neocortex may promote folding over a more prolonged time frame. This is faster in our *in vitro* system due to the increase in HLC levels, after the addition of the recombinant proteins, which could result in a faster rearrangement of the ECM environment and increased CD168 signaling.

Instead of replicating aspects of physiological folding such as proliferation, HLC-induced folding may instead highlight additional factors required for fold formation *in vivo*; the mechanics and signaling of the ECM. Addition of HLC to the human neocortex led to increased HA within the CP. This could create an environment permissive to fold formation, as HA is known to facilitate both the migration of cells and tissue morphogenesis via the RHAMM/CD168 receptor and loosening of the cell-ECM environment (Margolis et al., 1975; Solis et al., 2012). This possible function of HA in the CP is in line with a recent finding that reducing intracellular adhesion between the newborn neurons in the lissencephalic mouse caused the formation of sulci in the CP (Del Toro et al, 2017). The increase of HA in the CP and triggering of the CD168-ERK1/2 pathway, downstream of the increase in local ECM stiffness detected by AFM, could cause the movement of cells away from the areas with lowest stiffness towards the neighboring, stiffer areas (as observed in other systems (Kim et al., 2018; Lange and Fabry, 2013)), where the formation of expanding gyri can be supported by the stiffer ECM environment. This expansion could be further supported by the increase in HA, as loss of HA from early embryos has been previously reported to reduce their size (Morriss-Kay et al., 1986). Further support for this comes from the reduction of inherent folds at 22 GW caused by the loss of HA, suggesting maintenance of HA is required in this initial stage of neocortex folding. This combination of HA, ECM stiffness and downstream CD168/ERK signaling could therefore enable the neocortex to self-organize and modulate the environment to be either permissive to folding or not, ensuring that the folds form in the correct place (a process tightly regulated in physiological development). The HLC-induced folding system we have shown could be a useful tool in which to study how the location and formation of folds is regulated, including if there are any feedback loops between various parts of the HA/stiffness/CD168/ERK pathway. In this context, it would be interesting to develop approaches to manipulate ECM stiffness in a HA-independent manner to examine if such increases in stiffness are still required for folding, or if a HA increase and signaling via CD168/ERK are sufficient to induce folding.

This fold-inducing function of HLC and HA does not appear to be a common mechanism among all gyrencephalic species, as HLC treatment did not cause folding in the ferret at any age examined. However, as it was able to induce some changes in ECM stiffness, as measured by AFM, we cannot exclude the possibility that some of the steps in the complex process leading to HLC-induced folding are also initiated in the ferret, but fail to result in folding due to the lack of other downstream factors. Although we observed a lack of

HAPLN1 staining in the E33 ferret neocortex, HAPLN1 was detected at both P9 and P15, suggesting the absence of HAPLN1 was not responsible for the lack of folding. It is also unlikely that this is due to differences in the sequence homology of the ferret HAPLN1 protein compared to human HAPLN1, as it retains a 100% homology of the two link domains, which are able to bind HA. However, we also observed HA is not required for folding in the ferret neocortex as it is in human; addition of hyals and a HAS inhibitor were unable to reduce the GI of P9 or P15 ferret neocortex in FSN cultures, in contrast to 22 GW human neocortex FSN cultures. This lack of requirement of HA is also reflected in the location of the HA receptor CD168, which was observed at a lower level and in a more uniform pattern in the ferret CP at these later stages (P9, P15; Figure S6D, E) compared to a higher level around the newly forming gyrus in 22 GW human neocortex (Figure 6B). Overall, these data suggest that HLC and HA do not play the same role in folding of the ferret neocortex, but it could be possible that other ECM components may have a similar role in folding in this system instead.

Taken together, these data suggest HLC-induced folding could provide a useful system in which to study various aspects of human NDDs. This is especially prevalent for those disorders that lack model systems that accurately replicate specific aspects of the disorder, for example abnormalities of neocortex folding observed in lissencephalies and polymicrogyria. While this manuscript was in preparation, a study was published investigating the physics of neuroepithelial organoid folding in organoids from WT and Lis 1 mutant cells (Karzbrun et al., 2018). Interestingly, these Lis 1 mutant organoids showed a reduction in folding within this system and a reduction in *Coll1a2* levels, suggesting a potential physiological role of *Coll1a2* in such folding disorders. Here we show that HLC-induced folding revealed known aspects of various other NDDs, including abnormal folding after PME but not 2p16.3 microdeletion. It also revealed a delay in response to HLC-treatment in DS neocortex. DS is known to be associated with delayed development of the CP at early stages, which then catches up later in development (Golden and Hyman, 1994; Haydar and Reeves, 2012). Our present observations could therefore provide a useful system in which to study the early developmental delays seen in DS, allowing the examination of differential responses of neurons within the CP of DS and non-affected neocortex tissue.

Overall, our study has identified that the ECM components HAPLN1, lumican, collagen I and HA, their modulation of local tissue stiffness and the HA receptor CD168 as additional key players in the induction of fold formation in the human neocortex. It may also provide a link between the genetic and mechanical models, as regulation of the ECM by altering expression of the components themselves or the enzymes that can modify them, can allow the cells to regulate their own mechanical environment. Although our HLC-induced folding may not recapitulate every aspect of physiological folding, it has allowed us to uncover, and prematurely activate, a novel ECM-driven mechanism that can regulate early aspects of human neocortical folding and could be used to provide further insight into human neocortical development and its associated disorders.

References and Notes

Albert, M., Kalebic, N., Florio, M., Lakshmanaperumal, N., Haffner, C., Brandl, H., Henry, I., and Huttner, W.B. (2017). Epigenome profiling and editing of neocortical progenitor cells during development. *The EMBO journal* 36, 2642-2658.

Annus, T., Wilson, L.R., Acosta-Cabronero, J., Cardenas-Blanco, A., Hong, Y.T., Fryer, T.D., Coles, J.P., Menon, D.K., Zaman, S.H., Holland, A.J., *et al.* (2017). The Down syndrome brain in the presence and absence of fibrillar beta-amyloidosis. *Neurobiol Aging* 53, 11-19.

Bae, B.I., Jayaraman, D., and Walsh, C.A. (2015). Genetic changes shaping the human brain. *Dev Cell* 32, 423-434.

Bae, B.I., Tietjen, I., Atabay, K.D., Evrony, G.D., Johnson, M.B., Asare, E., Wang, P.P., Murayama, A.Y., Im, K., Lisgo, S.N., *et al.* (2014). Evolutionarily dynamic alternative splicing of GPR56 regulates regional cerebral cortical patterning. *Science* 343, 764-768.

Barkovich, A.J., Guerrini, R., Kuzniecky, R.I., Jackson, G.D., and Dobyns, W.B. (2012). A developmental and genetic classification for malformations of cortical development: update 2012. *Brain* 135, 1348-1369.

Bayly, P.V., Taber, L.A., and Kroenke, C.D. (2014). Mechanical forces in cerebral cortical folding: a review of measurements and models. *J Mech Behav Biomed Mater* 29, 568-581.

Binette, F., Cravens, J., Kahoussi, B., Haudenschild, D.R., and Goetinck, P.F. (1994). Link protein is ubiquitously expressed in non-cartilaginous tissues where it enhances and stabilizes the interaction of proteoglycans with hyaluronic acid. *J Biol Chem* 269, 19116-19122.

Borrell, V. (2018). How Cells Fold the Cerebral Cortex. *J Neurosci* 38, 776-783.

Casini, P., Nardi, I., and Ori, M. (2010). RHAMM mRNA expression in proliferating and migrating cells of the developing central nervous system. *Gene Expr Patterns* 10, 93-97.

Dahlstrand, J., Lardelli, M. & Lendahl, U. (1995). Nestin mRNA expression correlates with the central nervous system progenitor cell state in many, but not all, regions of developing central nervous system. *Dev Brain Res* 84, 109-129.

De Juan Romero, C., Bruder, C., Tomasello, U., Sanz-Anquela, J.M., and Borrell, V. (2015). Discrete domains of gene expression in germinal layers distinguish the development of gyrencephaly. *The EMBO journal* 34, 1859-1874.

Dehay, C., Kennedy, H., and Kosik, K.S. (2015). The outer subventricular zone and primate-specific cortical complexification. *Neuron* 85, 683-694.

Dzwonek, J., and Wilczynski, G.M. (2015). CD44: molecular interactions, signaling and functions in the nervous system. *Front Cell Neurosci* 9, 175.

Fernandez, V., Llinares-Benadero, C., and Borrell, V. (2016). Cerebral cortex expansion and folding: what have we learned? *The EMBO journal* 35, 1021-1044.

Fietz, S.A., Kelava, I., Vogt, J., Wilsch-Brauninger, M., Stenzel, D., Fish, J.L., Corbeil, D., Riehn, A., Distler, W., Nitsch, R., *et al.* (2010). OSVZ progenitors of human and ferret

neocortex are epithelial-like and expand by integrin signaling. *Nature neuroscience* *13*, 690-699.

Fietz, S.A., Lachmann, R., Brandl, H., Kircher, M., Samusik, N., Schroder, R., Lakshmanaperumal, N., Henry, I., Vogt, J., Riehn, A., *et al.* (2012). Transcriptomes of germinal zones of human and mouse fetal neocortex suggest a role of extracellular matrix in progenitor self-renewal. *Proceedings of the National Academy of Sciences of the United States of America* *109*, 11836-11841.

Florio, M., Albert, M., Taverna, E., Namba, T., Brandl, H., Lewitus, E., Haffner, C., Sykes, A., Wong, F.K., Peters, J., *et al.* (2015). Human-specific gene ARHGAP11B promotes basal progenitor amplification and neocortex expansion. *Science* *347*, 1465-1470.

Florio, M., and Huttner, W.B. (2014). Neural progenitors, neurogenesis and the evolution of the neocortex. *Development* *141*, 2182-2194.

Fraser, J.R., Laurent, T.C., and Laurent, U.B. (1997). Hyaluronan: its nature, distribution, functions and turnover. *J Intern Med* *242*, 27-33.

Golden, J.A., and Hyman, B.T. (1994). Development of the superior temporal neocortex is anomalous in trisomy 21. *J Neuropathol Exp Neurol* *53*, 513-520.

Graham, H.K., Hodson, N.W., Hoyland, J.A., Millward-Sadler, S.J., Garrod, D., Scothern, A., Griffiths, C.E., Watson, R.E., Cox, T.R., Erler, J.T., *et al.* (2010). Tissue section AFM: In situ ultrastructural imaging of native biomolecules. *Matrix Biol* *29*, 254-260.

Haydar, T.F., and Reeves, R.H. (2012). Trisomy 21 and early brain development. *Trends Neurosci* *35*, 81-91.

Hoogendoorn, R.J., Wuisman, P.I., Smit, T.H., Everts, V.E., and Helder, M.N. (2007). Experimental intervertebral disc degeneration induced by chondroitinase ABC in the goat. *Spine (Phila Pa 1976)* *32*, 1816-1825.

Hung, D.T., Jamison, T.F., and Schreiber, S.L. (1996). Understanding and controlling the cell cycle with natural products. *Chem Biol* *3*, 623-639.

Hutter, J.L., and Bechhoefer, J. (1993). Calibration of Atomic-Force Microscope Tips (Vol 64, Pg 1868, 1993). *Rev Sci Instrum* *64*, 3342-3342.

Jablonski, S.A., Williams, M.T., and Vorhees, C.V. (2016). Mechanisms involved in the neurotoxic and cognitive effects of developmental methamphetamine exposure. *Birth Defects Res C Embryo Today* *108*, 131-141.

Karzbrun, E., Kshirsagar, A., Cohen, S.R., Hanna, J.H., and Reiner, O. (2018). Human Brain Organoids on a Chip Reveal the Physics of Folding. *Nat Phys* *14*, 515-522.

Kim, M.C., Silberberg, Y.R., Abeyaratne, R., Kamm, R.D., and Asada, H.H. (2018). Computational modeling of three-dimensional ECM-rigidity sensing to guide directed cell migration. *Proc Natl Acad Sci U S A* *115*, E390-E399.

- Krieg, M., Arboleda-Estudillo, Y., Puech, P.H., Kafer, J., Graner, F., Muller, D.J., and Heisenberg, C.P. (2008). Tensile forces govern germ-layer organization in zebrafish. *Nat Cell Biol* 10, 429-436.
- Kroenke, C.D., and Bayly, P.V. (2018). How Forces Fold the Cerebral Cortex. *J Neurosci* 38, 767-775.
- Lange, J.R., and Fabry, B. (2013). Cell and tissue mechanics in cell migration. *Exp Cell Res* 319, 2418-2423.
- Lewitus, E., Kelava, I., and Huttner, W.B. (2013). Conical expansion of the outer subventricular zone and the role of neocortical folding in evolution and development. *Front Hum Neurosci* 7, 424.
- Lewitus, E., Kelava, I., Kalinka, A.T., Tomancak, P., and Huttner, W.B. (2014). An adaptive threshold in mammalian neocortical evolution. *PLoS Biol* 12, e1002000.
- Li, Y., Muffat, J., Omer, A., Bosch, I., Lancaster, M.A., Sur, M., Gehrke, L., Knoblich, J.A., and Jaenisch, R. (2016). Induction of Expansion and Folding in Human Cerebral Organoids. *Cell Stem Cell*.
- Lian, G., and Sheen, V.L. (2015). Cytoskeletal proteins in cortical development and disease: actin associated proteins in periventricular heterotopia. *Front Cell Neurosci* 9, 99.
- Livak, K.J., and Schmittgen, T.D. (2001). Analysis of relative gene expression data using real-time quantitative PCR and the 2(-Delta Delta C(T)) Method. *Methods* 25, 402-408.
- Lui, J.H., Hansen, D.V., and Kriegstein, A.R. (2011). Development and evolution of the human neocortex. *Cell* 146, 18-36.
- Lynn, B.D., Li, X., Cattini, P.A., Turley, E.A., and Nagy, J.I. (2001). Identification of sequence, protein isoforms, and distribution of the hyaluronan-binding protein RHAMM in adult and developing rat brain. *J Comp Neurol* 439, 315-330.
- Margolis, R.U., Margolis, R.K., Chang, L.B., and Preti, C. (1975). Glycosaminoglycans of brain during development. *Biochemistry* 14, 85-88.
- Masuda, K., Toda, T., Shinmyo, Y., Ebisu, H., Hoshiba, Y., Wakimoto, M., Ichikawa, Y., and Kawasaki, H. (2015). Pathophysiological analyses of cortical malformation using gyrencephalic mammals. *Sci Rep* 5, 15370.
- Matsumoto, N., Shinmyo, Y., Ichikawa, Y., and Kawasaki, H. (2017). Gyrification of the cerebral cortex requires FGF signaling in the mammalian brain. *Elife* 6.
- Miller, J.A., Ding, S.L., Sunkin, S.M., Smith, K.A., Ng, L., Szafer, A., Ebbert, A., Riley, Z.L., Royall, J.J., Aiona, K., *et al.* (2014). Transcriptional landscape of the prenatal human brain. *Nature* 508, 199-206.
- Miron-Mendoza, M., Seemann, J., and Grinnell, F. (2010). The differential regulation of cell motile activity through matrix stiffness and porosity in three dimensional collagen matrices. *Biomaterials* 31, 6425-6435.

- Molyneaux, B.J., Arlotta, P., Menezes, J.R., and Macklis, J.D. (2007). Neuronal subtype specification in the cerebral cortex. *Nat Rev Neurosci* 8, 427-437.
- Morriss-Kay, G.M., Tuckett, F., and Solursh, M. (1986). The effects of Streptomyces hyaluronidase on tissue organization and cell cycle time in rat embryos. *J Embryol Exp Morphol* 98, 59-70.
- Mota, B., and Herculano-Houzel, S. (2015). BRAIN STRUCTURE. Cortical folding scales universally with surface area and thickness, not number of neurons. *Science* 349, 74-77.
- Naba, A., Clauser, K.R., Hoersch, S., Liu, H., Carr, S.A., and Hynes, R.O. (2012). The matrisome: in silico definition and in vivo characterization by proteomics of normal and tumor extracellular matrices. *Mol Cell Proteomics* 11, M111 014647.
- Nagy, J.I., Hacking, J., Frankenstein, U.N., and Turley, E.A. (1995). Requirement of the hyaluronan receptor RHAMM in neurite extension and motility as demonstrated in primary neurons and neuronal cell lines. *J Neurosci* 15, 241-252.
- Nowakowski, T.J., Bhaduri, A., Pollen, A.A., Alvarado, B., Mostajo-Radji, M.A., Di Lullo, E., Haeussler, M., Sandoval-Espinosa, C., Liu, S.J., Velmeshev, D., *et al.* (2017). Spatiotemporal gene expression trajectories reveal developmental hierarchies of the human cortex. *Science* 358, 1318-1323.
- Parrini, E., Conti, V., Dobyns, W.B., and Guerrini, R. (2016). Genetic Basis of Brain Malformations. *Mol Syndromol* 7, 220-233.
- Pollen, A.A., Nowakowski, T.J., Chen, J., Retallack, H., Sandoval-Espinosa, C., Nicholas, C.R., Shuga, J., Liu, S.J., Oldham, M.C., Diaz, A., *et al.* (2015). Molecular Identity of Human Outer Radial Glia during Cortical Development. *Cell* 163, 55-67.
- Pollen, A.A., Nowakowski, T.J., Shuga, J., Wang, X., Leyrat, A.A., Lui, J.H., Li, N., Szpankowski, L., Fowler, B., Chen, P., *et al.* (2014). Low-coverage single-cell mRNA sequencing reveals cellular heterogeneity and activated signaling pathways in developing cerebral cortex. *Nat Biotechnol* 32, 1053-1058.
- Rakic, P. (2009). Evolution of the neocortex: a perspective from developmental biology. *Nat Rev Neurosci* 10, 724-735.
- Reillo, I., de Juan Romero, C., Garcia-Cabezas, M.A., and Borrell, V. (2011). A role for intermediate radial glia in the tangential expansion of the mammalian cerebral cortex. *Cereb Cortex* 21, 1674-1694.
- Reiner, O. (1999). The unfolding story of two lissencephaly genes and brain development. *Mol Neurobiol* 20, 143-156.
- Richman, D.P., Stewart, R.M., Hutchinson, J.W., and Caviness, V.S., Jr. (1975). Mechanical model of brain convolitional development. *Science* 189, 18-21.
- Rilla, K., Pasonen-Seppanen, S., Rieppo, J., Tammi, M., and Tammi, R. (2004). The hyaluronan synthesis inhibitor 4-methylumbelliferone prevents keratinocyte activation and epidermal hyperproliferation induced by epidermal growth factor. *J Invest Dermatol* 123, 708-714.

Saito, T., Dai, T., and Asano, R. (2013). The hyaluronan synthesis inhibitor 4-methylumbelliferone exhibits antitumor effects against mesenchymal-like canine mammary tumor cells. *Oncol Lett* 5, 1068-1074.

Schaefer, L., and Iozzo, R.V. (2008). Biological functions of the small leucine-rich proteoglycans: from genetics to signal transduction. *J Biol Chem* 283, 21305-21309.

Schenk, J., Wilsch-Brauninger, M., Calegari, F., and Huttner, W.B. (2009). Myosin II is required for interkinetic nuclear migration of neural progenitors. *Proceedings of the National Academy of Sciences of the United States of America* 106, 16487-16492.

Shinmyo, Y., Terashita, Y., Dinh Duong, T.A., Horiike, T., Kawasumi, M., Hosomichi, K., Tajima, A., and Kawasaki, H. (2017). Folding of the Cerebral Cortex Requires Cdk5 in Upper-Layer Neurons in Gyrencephalic Mammals. *Cell Rep* 20, 2131-2143.

Smart, I.H., Dehay, C., Giroud, P., Berland, M., and Kennedy, H. (2002). Unique morphological features of the proliferative zones and postmitotic compartments of the neural epithelium giving rise to striate and extrastriate cortex in the monkey. *Cerebral Cortex* 12, 37-53.

Solis, M.A., Chen, Y.H., Wong, T.Y., Bittencourt, V.Z., Lin, Y.C., and Huang, L.L. (2012). Hyaluronan regulates cell behavior: a potential niche matrix for stem cells. *Biochem Res Int* 2012, 346972.

Stahl, R., Walcher, T., De Juan Romero, C., Pilz, G.A., Cappello, S., Irmeler, M., Sanz-Aquela, J.M., Beckers, J., Blum, R., Borrell, V., *et al.* (2013). *Trnp1* regulates expansion and folding of the Mammalian cerebral cortex by control of radial glial fate. *Cell* 153, 535-549.

Stenzel, D., Wilsch-Brauninger, M., Wong, F.K., Heuer, H., and Huttner, W.B. (2014). Integrin α v β 3 and thyroid hormones promote expansion of progenitors in embryonic neocortex. *Development* 141, 795-806.

Sun, T., and Hevner, R.F. (2014). Growth and folding of the mammalian cerebral cortex: from molecules to malformations. *Nat Rev Neurosci* 15, 217-232.

Tallinen, T., Chung, J.Y., Biggins, J.S., and Mahadevan, L. (2014). Gyrfication from constrained cortical expansion. *Proc Natl Acad Sci U S A* 111, 12667-12672.

Tallinen, T., Chung, J.Y., Rousseau, F., Girard, N., Lefevre, J., and Mahadevan, L. (2016). On the growth and form of cortical convolutions. *Nature Physics* 12, 588-593.

Trochon, V., Mabilat-Pragnon, C., Bertrand, P., Legrand, Y., Soria, J., Soria, C., Delpech, B., and Lu, H. (1997). Hyaluronectin blocks the stimulatory effect of hyaluronan-derived fragments on endothelial cells during angiogenesis in vitro. *FEBS Lett* 418, 6-10.

Uhlen, M., Fagerberg, L., Hallstrom, B.M., Lindskog, C., Oksvold, P., Mardinoglu, A., Sivertsson, A., Kampf, C., Sjostedt, E., Asplund, A., *et al.* (2015). Proteomics. Tissue-based map of the human proteome. *Science* 347, 1260419.

van Oers, R.F., Rens, E.G., LaValley, D.J., Reinhart-King, C.A., and Merks, R.M. (2014). Mechanical cell-matrix feedback explains pairwise and collective endothelial cell behavior in vitro. *PLoS Comput Biol* 10, e1003774.

Vinas-Jornet, M., Esteba-Castillo, S., Gabau, E., Ribas-Vidal, N., Baena, N., San, J., Ruiz, A., Coll, M.D., Novell, R., and Guitart, M. (2014). A common cognitive, psychiatric, and dysmorphic phenotype in carriers of NRXN1 deletion. *Mol Genet Genomic Med* 2, 512-521.

Wong, F.K., Haffner, C., Huttner, W.B., and Taverna, E. (2014). Microinjection of membrane-impermeable molecules into single neural stem cells in brain tissue. *Nat Protoc* 9, 1170-1182.

Zhang, S., Chang, M.C., Zylka, D., Turley, S., Harrison, R., and Turley, E.A. (1998). The hyaluronan receptor RHAMM regulates extracellular-regulated kinase. *J Biol Chem* 273, 11342-11348.

Zhang, Z.N., Freitas, B.C., Qian, H., Lux, J., Acab, A., Trujillo, C.A., Herai, R.H., Nguyen Huu, V.A., Wen, J.H., Joshi-Barr, S., *et al.* (2016). Layered hydrogels accelerate iPSC-derived neuronal maturation and reveal migration defects caused by MeCP2 dysfunction. *Proc Natl Acad Sci U S A* 113, 3185-3190.

Zilles, K., Armstrong, E., Schleicher, A., and Kretschmann, H.J. (1988). The human pattern of gyrification in the cerebral cortex. *Anat Embryol* 179, 173-179.

Zilles, K., Palomero-Gallagher, N., and Amunts, K. (2013). Development of cortical folding during evolution and ontogeny. *Trends Neurosci* 36, 275-284.

Acknowledgments

We apologize to all researchers whose work could not be cited due to space limitation. We are grateful to the Services and Facilities of the MPI-CBG for the outstanding support provided, notably Jussi Helppi and his team of the Animal Facility, Holger Brandl and Lena Herseman from the Scientific Computing Facility and Jan Pechyl and his team of the Light Microscopy Facility. We are also grateful to Andreas Dahl and Suzanne Reinhardt from the Deep Sequencing Group, and Hella Hartman from the Light Microscopy Facility, both at the Centre for Regenerative Therapies Dresden (CRTD). We would also like to thank Dianne Gerrelli, Steve Lisgo and their teams at the HDBR along with James Nicoll and his team at BRAIN UK for the invaluable support from these resources, Robert Lachmann for providing human neocortical samples for the pilot experiments, Carsten Werner and Jens Friedrichs from the IPF for their assistance and expertise with the AFM experiments. We thank Mareike Albert for advice with qPCR, Elena Taverna for useful suggestions, Romy Schuster for help with immunostaining, and members of the Huttner lab for critical discussion and review of the manuscript. B.N. would like to thank the Wellcome Trust for the Sir Henry Wellcome Postdoctoral Fellowship. W.B.H. was supported by grants from the DFG (SFB 655, A2) and the ERC (250197). The supplementary materials contain additional data. RNA-seq raw data have been deposited with the Gene Expression Omnibus under accession codes GSE106640.

Contributions

K.R.L and W.B.H. designed the study, analyzed the data and wrote the manuscript, with input from the other authors. K.R.L. performed and analyzed the experiments, collaborating with B.N. in the AFM and hydrogel experiments, with M.F. in the transcriptome analyses, and with N.K. and B.L. in the ferret experiments. A.K. and P.W. provided human neocortex tissue. W.B.H. supervised the study.

Competing interests

The authors declare no competing financial interests.

Figure Legends

Figure 1. HAPLN1, lumican and collagen I selection and IF.

(A) Stepwise exclusion parameters to the datasets of core matrisome genes (Naba et al., 2012) that were differentially expressed between 13-17 GW human neural progenitor cells (NPCs) than E14.5 mouse NPCs and E9.5 mouse neuroepithelial cells (NECs), to home-in on genes specifically expressed in human NPCs that were downregulated in mouse neural development. See also Table 1.

(B) DAPI staining (blue) and either HAPLN1, lumican or collagen I IF (grey, as indicated) of 13 GW human neocortex (huNcx) (top row) and E14.5 mouse neocortex (bottom row). Scale bars: 200 μ m.

Figure 2. Addition of the ECM components HLC to 11-14 GW human neocortex in organotypic slice culture and FFTC induces in vitro folding of the CP.

Organotypic slice cultures (**A, C, D**) and FFTCs (**B, E-I**) of 11-14 GW huNcx subjected to treatment for 24 h.

(**A**) DAPI staining of 13 GW human neocortex embedded in collagen I alone (Control), with addition of HAPLN1 and lumican (HAPLN1 + lumican) and with only HAPLN1 (HAPLN1).

(**A, B**) Lines on left of panel indicate the CP and the ventricular surface (VS).

(**B**) DAPI staining of 13 GW huNcx in FFTC subjected to control and HLC-treatment.

(**C**) Quantification of Gyrencephalic Index (GI) of 11-14 GW huNcx in FFTC subjected to the indicated treatments. *, $P=0.04$; **, $P=0.0015$.

(**D, E**) DAPI staining (blue) and laminin IF (red) of CP of 13 GW huNcx in organotypic slice cultures (**D**) and FFTC (**E**).

(**F**) Quantification of GI of 11-14 GW huNcx in FFTC subjected to control and HLC-treatment. ***, $P < 0.0001$.

(**G**) DAPI staining (blue) and nestin IF (grey) of 13 GW huNcx. Dashed boxes delineate panels on right.

(**H**) Quantification of GI in 11-14 GW huNcx in FFTC subjected to the indicated conditions. ***, $P=0.0008$.

(**I**) Still images at the indicated time points of time-lapse imaging of 12 GW huNcx in organotypic slice culture subjected to control (top) and HLC-treatment (bottom). Arrowheads indicate sulcus between forming gyri.

(**A, B, D, E, G, I**) Scale bars: (**A, B, D, E, I**) 200 μm , (**G**) 50 μm . (**B**) and (**G**) are independent experiments (ind. exp.).

(**C, F, H**) Statistical tests; one-way ANOVA (**C, H**), unpaired Student's t -test (**F**). Error bars, SD; ns, $P > 0.05$. Data points in (**C, H**) 3-4 ind. exp. (1 fetus/exp.) with 1-2 slice (**C**) or FFTCs (**H**) per condition per fetus, and in (**F**) 8 ind. exp. (1 fetus/exp.) with 1-3 FFTCs per condition per fetus.

Figure 3. HLC IF in 18 GW human neocortex, and HLC and HA IF in 22 GW and 38 GW human neocortex CP.

(A) DAPI staining (blue) and either HAPLN1, lumican or collagen 1 IF (grey, as indicated) of 18 GW huNcx. Yellow boxes delineate areas in panels on right.

(B, C) DAPI staining (blue) and co- IF of HA (green) and either HAPLN1, lumican or collagen 1 (grey, as indicated) of 22 GW CP (B), containing a nascent, inherent fold, and 38 GW CP (C) in the gyrus and sulcus (as indicated). (C, far left) Image of 38 GW section used for CP images (right). Yellow dashed line delineates CP surface, blue arrows indicate areas imaged.

(A-B) Scale bars: (A) 200 μm , (B) 500 μm and (C) 50 μm for CP insets and 1 cm for entire section image.

Figure 4. HLC-induced folding increases and requires HA at 11-14 GW and 22 GW.

(A, A') DAPI staining (blue) and double IF for HAPLN1 (yellow) and HA (red) of 14 GW huNcx in FFTC subjected to control (top) and HLC-treatment (bottom) for 24 h. Top and bottom dashed boxes delineate CP and VZ panels, respectively, in A'. White dashed lines outline unfolded (control) and folded (HLC-treatment) CP surface. (B) Quantification of the CP/VZ ratio of HA immunoreactivity of 11-14 GW huNcx in FFTC subjected to the indicated treatments for 24 h. ***, $P=0.0009$; **, $P=0.0032$. (C) Quantification of the CP/VZ ratio of HA immunoreactivity of 13-15 GW huNcx in FFTC subjected to control and HLC-treatment for 8 and 16 h. *, $P=0.0128$ (8 h); *, $P=0.0394$ (16 h).

(D) DAPI staining (blue) and HA IF (red) of 12 GW huNcx in FFTC subjected to control (left), HLC-treatment (middle) and HLC-treatment in the presence of hyals (right) for 24 h. Dashed boxes delineate panels below.

(E) Quantification of GI of 12-14 GW huNcx in FFTC subjected to the indicated treatments for 24 h, except for the condition *HLC-treatment + hyaluronidases @ 24 h* (HLC-treatment for 48 h with addition of hyals at 24 h). ***, $P=<0.0001$ (control vs. HLC-treatment) and $P=0.0005$ (control vs. HLC-treatment + chondABC); **, $P=<0.0021$.

(F) Quantification of GI of 14-18 GW huNcx in FFTC subjected to indicated treatments. ***, $P=0.0008$, $P=0.0008$.

(G-K) 22 GW huNcx in FFTC was subjected to the indicated treatments for 4 days, except for the condition *non-cultured* in (H). (G, H) Quantification of GI. *, $P=0.0124$; **, $P=0.0066-0.0074$; ***, $P=0.0009$. (I-K) DAPI staining of the CP upon control (I top, J left, K left), HLC-treatment (I middle, J right) and hyals plus HAS inhibitor (I right, K right). White dashed lines outline unfolded or folded CP surface; arrowheads indicate sulcus.

(A, A', D, I, J, K) Scale bars: (A, D, E) 200 μm , (A' and insert in D) 50 μm and (I-K) 500 μm . (B, C, E-H) Statistical tests; one-way ANOVA (B, E-H), two-way ANOVA (C). Error bars, SD; ns, $P>0.05$. Data points in (B) 8 ind. exp. (1 fetus/exp.) with 1-3 FFTCs per condition per fetus; in (F) 5-6 ind. exp. (1 fetus/exp.) with 1-3 FFTCs per condition per fetus; in (G) 3 ind. exp. (1 fetus/exp.) with 1 FFTC/exp.

Figure 5. HLC-treatment replicates certain aspects of 22 GW physiological nascent folds and increases ECM stiffness.

(**A, B**) DAPI staining (blue) and double IF for TBR1 (yellow) and CTIP2 (red) of 22 GW huNcx not subjected to culture (**A**). Note the nascent fold of the CP, and 15 GW huNcx in FFTC subjected to control and HLC-treatment (**B**) (2 examples shown).

(**C-E**) 11-14 GW huNcx in FFTC subjected to control and HLC-treatment for 24 h. (**C**) Representative images showing DAPI staining of 13 GW huNcx CP of control (left), CP sulcus upon HLC-treatment (middle), and CP gyrus upon HLC-treatment (right). (**D**) Frequency distribution histogram for the distance between nuclei within the CP. (**E**) Quantification of the distance between nuclei within the CP. Data are presented in a whisker plot showing the minimum, mean and maximum values. *, $P=0.02$ (control vs. gyrus), $P=0.0148$ (sulcus vs. gyrus).

(**F-H**) AFM measurements in sections of 13 GW (**G, H**) and 12-14 GW (**F**) huNcx in FFTC subjected to control (**G, H**, left; **F**) and HLC-treatment (**G, H**, right; **F**) for 16 h (**G**) and 24 h (**H, F**), and of non-cultured 22 GW huNcx (**I**). Each heatmap square in (**G, H, I**) shows 9 Young's modulus values in the position the measurement was taken (see range of values from blue (lowest) to yellow (highest)). White dashed lines in (**G, H, I**) outline unfolded or folded CP surface; arrowheads indicate sulci. (**F**) Quantification of AFM measurements in 12-14 GW huNcx samples in FFTC (1 FFTC/condition). *, $P=0.0198$. (**J**) Quantification of the range of AFM measurements in 22 GW huNcx subjected to the indicated treatments for 4 days. Y axis represents the range of the Young's modulus values measured (in Pa).

(**A, B, C, G, H, I**) Scale bars: (**A, B, D, J**) 200 μm , (**C**) 50 μm and (**I**) 500 μm . (**E, F**) Statistical test; one-way ANOVA. Error bars, SEM. Data points in (**D, E**), 4 ind. exp. (1 fetus/exp.) with 1 FFTC per condition per fetus, in (**J**) 2 ind. exp. (1 fetus/exp.) with 1 FFTC per condition per fetus.

Figure 6. HLC-induced folding requires the HA-receptor CD168 and downstream ERK signaling.

(A, B) DAPI staining (blue) and triple IF for HA (green) and the HA-receptors CD168 (grey) and CD44 (magenta) in non-cultured 13 GW huNcx wall (A) and 22 GW human CP (B).

(C) DAPI staining of 14 GW huNcx in FFTC subjected to control (top left), HLC-treatment (top right), HLC-treatment plus CD44 antibody (lower left) and HLC-treatment plus CD168 antibody (lower right) for 24 h.

(D) Quantification of GI in 12-15 GW huNcx in FFTC subjected to the indicated treatments for 24 h. **, $P=0.0092$; *, $P=0.108$.

(E) Quantification of the CP/VZ ratio of HA immunoreactivity of 11-14 GW huNcx in FFTC subjected to the indicated treatments for 24 h. *, $P<0.05$.

(F) Quantification of pERK immunoreactivity in the CP relative to control of 12-15 GW huNcx in FFTC subjected to the indicated treatments for 24 h, *, $P=0.0194$.

(G) Quantification of pERK immunoreactivity in the CP relative to control of 12-15 GW huNcx in FFTC subjected to the indicated treatments for 8 and 24 h. Blue dashed line indicates control (set to 1.0).

(H) Quantification of the ratio of pERK immunoreactivity in gyri compared to their neighboring sulci of 12-16 GW huNcx in FFTC subjected to HLC-treatment for 24 h. Blue dashed line indicates control (set to 1.0).

(I) Quantification of pERK immunoreactivity in the CP of 13-14 GW huNcx in FFTC subjected to the indicated treatments for 24 h, relative to control indicated by the blue dashed line (set to 1.0). *, $P=0.0308$.

(J) Quantification of GI in 12-16 GW huNcx in FFTC subjected to control, HLC-treatment and HLC-treatment plus ERK inhibitor for 24 h. **, $P=0.0066$ (control vs, HLC-treatment), $P=0.0074$ (HLC-treatment vs. HLC-treatment + ERK inhibitor).

(K) DAPI staining (blue) and pERK IF (grey) of 16 GW huNcx in FFTC subjected to control, HLC-treatment and HLC-treatment plus ERK inhibitor for 24 h.

(A-C, K) Scale bars: 200 μm .

(D-G, I, J) Statistical test; one-way ANOVA (D-F, I) and Student's *t*-test (G, J). Error bars, SD; ns, $P>0.05$. Data points in (D-J) 3 ind. exp. (1 fetus/exp.) with 1 FFTC per condition per fetus.

Figure 7. HLC-induced folding is perturbed in specific human neocortex samples with NDDs.

(A) DAPI staining of the CP of 16 GW huNcx with DS in FFTC subjected to control (left) and HLC-treatment (right) for 24 h.

(B) Quantification of GI in 12-17 GW huNcx samples with altered neocortex development as indicated, subjected to control (open circles) and HLC-treatment (filled circles) in FFTC for 24 h. ***, $P=0.0005$.

(C-E) DAPI staining (blue) and HA IF (green) in 14 GW DS (C), 12 GW PME (D) and 2p16.3 microdeletion (E) huNcx in FFTC subjected to control (left) and HLC treatment (right).

(F-I) 21 GW DS sample subjected to control (F, top, I left) HLC-treatment (F, middle, I, right) and the indicated HA level-reducing treatment (F, bottom) for 4 days. (F) White dashed lines outline the unfolded or folded CP surface; white asterisk indicates tear in CP (bottom). (G) Quantification of GI in 21 GW huNcx with DS in FFTC subjected to the indicated treatments for 4 days. **, $P=0.0014-0.0076$.

(H) Quantification of the CP/VZ ratio of HA immunoreactivity of 12-16 GW and 21 GW huNcx with the indicated NDDs in FFTC subjected to HLC-treatment for 24 h (12-16 GW) or 4 days (21 GW). Bars indicate one fetal sample per indicated NDD, therefore values are shown relative to control (control set to 1.0) and without statistical analysis. For each sample, an average of 3 cryosections per condition were analyzed. Color of the bars indicate huNcx samples where GI was not significantly increased (white) or was significantly increased after HLC-treatment (grey). (I) DAPI staining and HA IF from CP of 21 GW DS sample subjected to control (left) and HLC-treatment (right).

(A, C-F, I) Scale bars: (A, F) 500 μm , (C-E) 200 μm , (I) 50 μm .

(B, G) Statistical test; two-way ANOVA (B), one-way ANOVA (G). Error bars, SD, ns = $P > 0.05$. Data points in (B, G) 1 ind. exp. (1 fetus/exp.) with 3-6 FFTCs per condition per fetus.

Table 1. 9 genes: Mouse NPCs no/low expression FPKM <1.

Gene ID	Mouse NECS	Mouse aRG	Mouse bRGs	Mouse bIPs	Mouse Neurons	Human aRG	Human bRG	Human Neurons
COL1A2	10.282964	0.171441	0.0415107	0.104064	0.115875	10.4022	4.27089	1.63804
HAPLN1	25.88738	0.103337	0.0826579	0.0368054	0.1021	8.0011	2.95787	0.618723
LUM	42.58198	0.11563	0.0597305	0.0444983	0.24573	4.41632	1.78397	0.53201
TINAG	2.761322	0.11633	0.124181	0.162185	0.168129	3.77847	3.24168	1.70318
COL3A1	4.96066	0.101161	0.0612023	0.0661498	0.0410923	3.43414	2.13655	1.27261
EGFLAM	3.076604	0.0654521	0.117693	0.239263	0.137794	1.50781	0.517271	0.150278
RSPO2	2.320142	0.0526038	0.0619082	0.0446231	0.239362	1.44148	0.968042	0.789062
PCOLCE2	22.2624	0.184318	0.0904057	0.277552	0.239362	0.86201	0.651806	0.504199
COL23A1	3.689042	0.295979	0.105298	0.101661	0.154592	0.252818	0.449853	0.0507757

Methods

CONTACT FOR REAGENT AND RESOURCE SHARING

Further information and requests for resources and reagents should be directed to and will be fulfilled by the Lead Contact, Wieland Huttner (huttner@mpi-cbg.de).

EXPERIMENTAL MODEL AND SUBJECT DETAILS

Tissue

Human tissue

Human fetal brain tissue was obtained from three sources. First, from the Klinik und Poliklinik für Frauenheilkunde und Geburtshilfe, Universitätsklinikum Carl Gustav Carus of the Technische Universität Dresden, following elective pregnancy termination and informed written maternal consents, and with approval of the local University Hospital Ethical Review Committees. The age of fetuses ranged from 11 to 13 GW as assessed by ultrasound measurements of crown-rump length and other standard criteria of developmental stage determination. The second source was the Human Development Biology Resource (HDBR). The human embryonic and fetal material was provided by the Joint MRC/Wellcome Trust (grant # 099175/Z/12/Z) Human Developmental Biology Resource (www.hdbbr.org). The HDBR provided fresh tissue from fetuses aged 13-22 GW, (13 GW, $n = 3$; 14 GW, $n = 11$; 15 GW, $n = 9$; 16 GW, $n = 2$; 18 GE, $n = 2$; 22 GW, $n = 3$). Several samples with neurodevelopmental defect were also obtained. A sample affected by methamphetamine abuse was obtained from the Klinik in Dresden (12 GW, $n = 1$), and the HDBR provided 5 samples with Down syndrome (12 GW, $n = 2$; 16 GW, $n = 1$; 17 GW, $n = 1$; 21 GW, $n = 1$) and 1 sample with a 2p16.3 microdeletion (16 GW, $n = 1$). Due to protection of data privacy, neither gender identity nor sex of the human fetuses of which neocortex tissue was obtained can be reported. Neither gender identity nor sex of the human fetuses is likely to be of relevance for the results obtained in the present study.

Human fetal brain tissue was dissected in PBS and used immediately for culture or fixation when obtained from Dresden. When obtained from HDBR, tissue was dissected and shipped in Hibernate E media (Gibco A1247601). Upon arrival, all tissue was cultured in slice culture medium (SCM - see the following section) for 2-3 h prior to any further manipulation. All tissue was fixed for at least 24 h at 4°C in 4% (wt/vol) paraformaldehyde (PFA) in 120 mM phosphate buffer (pH 7.4). The HDBR also provided fixed neocortical material from 3

fetuses aged 13, 18, 22 and 24 GW. This tissue was placed into 4% PFA (wt/vol) in 120 mM phosphate buffer immediately after dissection and shipped within this fixative (fixation was for at least 24 h). The third source provided fixed tissue sections (38 GW). These were obtained from University Hospital Southampton as part of the UK Brain Archive Information Network (BRAIN UK) which is funded by the Medical Research Council and Brain Tumour Research. Sample size was determined from the number of fetuses from whom neocortex tissue was obtained, and is indicated in the relevant figure legends.

Ferret tissue

Timed-pregnant ferrets were obtained from Marshall BioResources and housed at the BMS of MPI-CBG. For the analysis of embryonic day (E) 33-36 ferret embryos, pregnant ferrets were deeply anesthetized by subcutaneous injection of ketamine (40 mg/kg) plus xylazine (2 mg/kg); the embryos were collected in PBS, and the adult ferret was then sacrificed by intracardiac injection of T-61 (0.3 ml/kg). Embryonic ferret neocortex was then used for the preparation of organotypic slice cultures or FFTCs (E33-36) or fixed immediately in 4% PFA in phosphate buffer. Postnatal day (P) 9 and P15 ferret pups were deeply anesthetized by intraperitoneal injection of ketamine (40 mg/kg) plus xylazine (2 mg/kg), and then either sacrificed by decapitation (followed by dissection in PBS for FFTC) or by intracardial perfusion using 4% PFA in phosphate buffer at 37°C. Perfusions were performed with additional anesthetization with 4% isoflurane.

Mouse tissue

All mice used were wild-type C57BL/6J OlaHsd. E0.5 was set at noon of the day on which the vaginal plug was observed. All experiments were performed in the dorsolateral neocortex of E14.5 embryos, and all images were acquired and analyzed from coronal sections of the frontal and parietal neocortex.

Mouse and ferret neocortical tissue for fixation, either prior to or after manipulation, was fixed for at least 24 h at 4°C in 4% (wt/vol) PFA in 120 mM phosphate buffer (pH 7.4).

All animal experimental procedures were designed and conducted in agreement with the German Animal Welfare Legislation. Animals used for this study were kept pathogen-free at the Biomedical Services Facility (BMS) of the MPI-CBG.

METHOD DETAILS

Organotypic slice cultures and free-floating tissue cultures

Organotypic neocortical slice cultures and free-floating tissue (FFT) neocortex cultures were performed as previously described (Fietz et al., 2012; Schenk et al., 2009; Wong et al., 2014). The media used for both types of cultures was slice culture medium (SCM): 84 ml of Neurobasal medium (Gibco, 21103049) supplemented with 10 ml rat serum (for mouse and ferret cultures) or 10 ml of KOSR (for human cultures, Gibco, 10828028), 1 ml glutamine (2 mM), 1 ml Penstrep (100x), 1 ml N-2 (100x) (Gibco, 17502048), 2 ml B-27 (50x) (Gibco, 17504044) and 1 ml of 1 M HEPES-NaOH, pH 7.2, to yield a final volume of 100 ml.

Briefly, for organotypic slice cultures, neocortical tissue was embedded in 3% low melting point agarose (Sigma, A2790), cut on a vibratome to 250 μm -thick slices, and embedded in a collagen I-based hydrogel (Cellmatrix type I-A, Kyowa chemical products, 631-00651) (Wong et al., 2014) before culture at 37°C in the presence of humidified 40% O₂ / 5% CO₂ /55% N₂. Hence, as all organotypic slice cultures were embedded in collagen I (100 μl per slice, except for live imaging, see below), this condition applies to the control. As indicated, recombinant human HAPLN1 (R&D, 2608-HP-025; 100 $\mu\text{g/ml}$ stock solution in PBS) and recombinant human lumican (R&D, 2846-LU-050; 200 $\mu\text{g/ml}$ stock solution in PBS) were added to the collagen I embedding solution (final collagen concentration 1.5 mg/ml in DMEM) to yield a final concentration of 5 $\mu\text{g/ml}$ each. Control received the equivalent volume of PBS. For the laminin and collagen IV condition, recombinant laminin-211 (BioLamina, LN211; 100 $\mu\text{g/ml}$ stock solution) and native human collagen IV (abcam, ab7536; 1 mg/ml stock solution) were added to the collagen I embedding solution to yield a final concentration of 5 $\mu\text{g/ml}$ each. The concentration of 5 $\mu\text{g/ml}$ was chosen for ECM components in light of previous reports using various ECM components in vitro (van Oers et al., 2014; Zhang et al., 2016). Each slice then received 1 ml of SCM followed by culture.

For FFTCs, tissue was manually cut to 2000-2500 μm -thick pieces (tangential dimension), placed into a rotating flask with 1.5 ml SCM, and incubated at 37°C in the presence of humidified 40% O₂ / 5% CO₂ /55% N₂. Control FFTCs had nothing added to the SCM. For the HLC-treatment condition, recombinant human HAPLN1 (R&D 2608-HP-025), recombinant human lumican (R&D 2846-LU-050) and native human collagen I (abcam

ab7533; 1 mg/ml stock solution) were added to the SCM. Each ECM component had a final concentration of 5 $\mu\text{g/ml}$.

Other conditions for FFTCs were as follows. For hyaluronidase experiments, a cocktail of hyaluronidases added to the SCM was used: hyaluronidase-type-1 (Sigma, H3506) at a final concentration of 50 $\mu\text{g/ml}$, hyaluronidase-type-IV (Sigma, H3884) at a final concentration of 50 $\mu\text{g/ml}$, and hyaluronidase-type-VI (Sigma, H3631) at a final concentration of 50 units/ml. To inhibit synthesis of HA, the HA synthase (HAS) inhibitor 4-methylumbelliferone (Sigma, M1381) was added to the SCM at a final concentration of 0.2 mM. Hyaluronidase and HAS inhibitor treatments were also applied in combination, as indicated. To target chondroitin sulfate glycosaminoglycan components of the ECM, chondroitinase ABC (Sigma, C3667) was added to the SCM at a final concentration of 0.2 units/ml. To inhibit proliferation, mitomycin C (Tocris, 3258/10) was added to the SCM at a final concentration of 10 $\mu\text{g/ml}$. To inhibit ERK activity, the selective ERK inhibitor FR 180204 (Tocris, 3706) was added to the SCM at a final concentration of 3 mM. The concentrations selected for the above enzymes and inhibitors were selected in light of previous reports (Hoogendoorn et al., 2007; Saito et al., 2013; Trochon et al., 1997).

In addition to the above, the following conditions for FFTCs were used. A soluble basement membrane extract, Geltrex (Gibco, A15696), was added to the SCM at a final concentration of 5 $\mu\text{g/ml}$. For ferret FFTCs as indicated, HA (1-3%, Advanced Biomatrix, 5011-3) was used at a final concentration of 10 $\mu\text{g/ml}$. This concentration was chosen to ensure that the HA would saturate the recombinant HAPLN1 added to the FFTCs (5 $\mu\text{g/ml}$). The CD44 antibody (abcam, ab25340) and the CD168 antibody (abcam, ab185728) were each added to the SCM at a final concentration of 30 $\mu\text{g/ml}$. For quantification of cells in S-phase, EdU was added to the SCM at a final concentration of 1 $\mu\text{g/ml}$ (Click-iT EdU Alexa Fluor 647 imaging kit, Invitrogen, C10340) 1 hour prior to fixation.

Cryosectioning and immunostaining

Fixed tissue for cryosectioning was infiltrated with 30% sucrose overnight at 4°C before being embedded in Tissue-Tek (Sakura Finetek) and stored at -20°C. Cryosections were cut at 20 μm and stored at -20 °C until required. Sections for immunostaining that required antigen retrieval were subjected to 10 mins at 95°C in citrate buffer (pH 6.1, Target Retrieval Solution, DakoCytomation). All sections were then treated with blocking solution (PBS

supplemented with 10% goat serum, containing a final concentration of 0.1% Triton X-100) for 30 mins before the addition of the primary and appropriate secondary antibodies, both diluted in blocking solution. The primary antibodies used were as follows: nestin (abcam, ab27952), HAPLN1 (abcam, ab181997), HA (abcam, ab53842), lumican (abcam, ab168348), Colla2 (abcam, ab96723), pVim (abcam, ab22651), CD168 (abcam, ab185728), CD44 (abcam, ab119348), CTIP2 (abcam, ab18465), TBR1 (abcam, ab31940), PCNA (Millipore, CBL407), phospho-p44/42 MAPK (Erk1/2) (cell signaling, 9101), Phospho-p90RSK (Ser380) (D3H11) (cell signaling, 11989) and Penta His-tag (Qiagen, 34660). All antibodies were used at a 1/100 dilution. The secondary antibodies used were conjugated to Alexa Fluor 488, 568 and 647 (Invitrogen), and all were used at 1/1000. EdU staining was performed using the Click-iT EdU Alexa Fluor 647 imaging kit (Invitrogen, C10340). All sections were counterstained with DAPI (Sigma, 1:1000) and mounted in Mowiol (Merck Biosciences). Sections were then imaged using a Zeiss LSM 700 inverted confocal microscope and a Zeiss Plan-Apochromat 20x 0.8 objective. For 22 GW human samples and P9 and P15 ferret samples, sections were first imaged using a Zeiss Axio Scan wide-field microscope and Zeiss Plan-Apochromat 10x 0.45 objective prior to selecting sections for imaging with the above confocal microscope. Images shown are maximum intensity projections of 11 optical sections from a 10 μ m z-stack.

Laser capture microdissection

Laser capture microdissection (LCM) was performed in a similar manner as described previously (21). Human fetal neocortex tissue was cultured for 16 h (FFTC) with and without HLC-treatment, immediately frozen on dry-ice, and stored at -80°C . The tissue was then embedded in Tissue-Tek and cut at 30 μ m sections on a cryostat. Cryosections were mounted onto nuclease-free MembraneSlide NF 1.0 PEN (Zeiss 415190-9081-000). Immediately prior to LCM, slides were rinsed for 30 sec in 70% (vol/vol) ice-cold ethanol, incubated for 30 sec in 1% cresyl violet in 100% (vol/vol) ethanol, and washed twice for 30 sec each in 100% (vol/vol) ethanol. Sections were then immediately subjected to LCM using an Axiovert 200M microscope equipped with a PALM LCM MicroBeam system (Zeiss) and a Zeiss Fluar 5x 0.25 objective. For each cryosection, multiple square or rectangular areas of the cortical plate were isolated, with an edge length of 350-400 μ m (tangential dimension) by 200-400 μ m (radial dimension), and collected using AdhesiveCap tubes (Zeiss 415190-9201-000). Three to four tubes were obtained per sample. Each tube received 350 μ l of RLT buffer (from the RNAeasy Mini kit Qiagen), was immediately stored on dry-ice and then transferred to -80°C .

RNAseq library preparation

Total RNA was extracted using the RNeasy Mini kit (Qiagen), and polyadenylated mRNA was enriched with the NEBNext Poly(A) mRNA Magnetic Isolation Module (New England Biolabs) according to the manufacturer's instructions. The cDNA and second strand synthesis as well as the library preparation (consisting of cDNA fragmentation, end repair, A-tailing, ligation of sequencing adapters, indexing by PCR amplification for 15 cycles) were performed using the NEBNext Ultra II Directional RNA Library Prep Kit Illumina (New England Biolabs). Libraries were purified using XP beads (Beckman Coulter), quantified by Fragment Analyzer (AATI) and subjected to Illumina 75-bp single end sequencing on the Illumina Nextseq500 platform providing a minimum of 21 Mio reads per sample.

Transcriptome data analysis

Reads were checked for their overall quality using FastQC (v0.11.2). Alignments of reads against the human genome reference assembly GRCh38 and quantification of genes of the Ensembl release v88 were done using STAR (v2.5.2b). For the verification of technical duplicates, duplicated reads identified using Picard MarkDuplicates (v2.10.2) were analyzed with dupRadar (v1.6.0). Differential gene expression analysis on raw counts was performed with DESeq2 (v1.16.1) using a cutoff first of $P < 0.01$ and then of $P < 0.05$. The resulting list of 438 differentially expressed genes obtained with the latter cutoff was tested for enrichment in GO terms and pathways (KEGG, Reactome) on a 1% q-value level.

qPCR

Total RNA was isolated using the RNeasy Mini kit (Qiagen) according to the manufacturer's guidelines. cDNA was synthesized using random hexamers and Superscript III Reverse Transcriptase (Life Technologies). qPCR was performed using the Light Cycler SYBR Green Master mix (Roche) on a Light Cycler 96 (Roche), using the following settings: 95°C for 15 min, followed by 40 cycles at 95°C for 30 sec, at 60°C for 30 sec and at 72°C for 30 sec. Fold change in mRNA levels of each gene was determined relative to *HPRT1* and then relative to control, using the $\Delta\Delta C_t$ method (Livak and Schmittgen, 2001). Primer sequences are provided in Table S2.

Atomic force microscopy

Atomic force microscopy (AFM) was used to determine the Young's moduli of various regions of the CP (i) in human 11-14 GW neocortex tissue after 8, 16 and 24 h of FFTC, (ii) in human 22 GW neocortex tissue that was frozen without fixation at the HDBR, shipped on dry-ice and stored at -80°C , and (iii) in ferret E33 neocortex tissue after 24 h of FFTC. To cut thin sections of the relatively soft human fetal neocortex that are required for AFM, and to be able to determine tissue stiffness preferentially with regard to ECM-cell interactions, samples underwent two freeze-thaw cycles as follows. Following FFTC, samples were frozen on dry-ice and stored at -80°C . The frozen FFT samples and the frozen human 22 GW neocortex tissue were thawed (completion of first freeze-thaw cycle), embedded in Tissue-Tek at room temperature, again frozen on dry-ice, and stored at -80°C . Cryosections were then cut at a thickness of $100\ \mu\text{m}$ and adhered to glass slides suitable for AFM (Superfrost Plus, Thermo Scientific). The samples were then stored at -20°C until analysis. Immediately prior to performing the AFM measurements, the cryosections were defrosted under laminar flow (completion of second freeze-thaw cycle) and air-dried before being gently submerged in PBS. The NanoWizard II AFM (JPK Instruments) was mounted on an Axio Observer D.1 microscope (Zeiss) to allow visualization of the cryosections and correct positioning of the AFM tip. Experiments were performed at room temperature (held at 21°C). AFM measurements were performed using silicon nitride cantilevers with a nominal spring constant of $80\ \text{mN/m}$ (PNP-TR-TL-Au; Nanoworld) with a $10\ \mu\text{m}$ diameter silica bead (Kisker Biotec GmbH) adhered to the tip as reported previously (Krieg et al., 2008). Spring constants were calibrated before measurements using the equipartition theorem (Hutter and Bechhoefer, 1993). For indentation measurements, force-distance curves were taken in closed loop, constant height mode with an approach and retract velocity of $5\ \mu\text{m s}^{-1}$, a contact force of $2\ \text{nN}$, and a z-length of $30\ \mu\text{m}$. Each data point was generated by taking 9 force-distance curves in a square shape of $30\ \mu\text{m} \times 30\ \mu\text{m}$ (see Fig. 3a, b, d). A minimum of three data points were taken for each cryosection, and a minimum of 3 cryosections were measured per piece of tissue. The Young's modulus (E) was calculated from the approach force-distance curves via the JPK Instruments data processing software. A Hertz fit was applied assuming a spherical indenter of radius (R) $5\ \mu\text{m}$, and a Poisson's ratio (ν) of 0.5 according to the following equation:

$$F = \frac{4}{3} * \frac{E}{1-\nu^2} * \sqrt{R} * \delta^{3/2}$$

where δ is the indentation and F is the force.

Live imaging

Live imaging was carried out on organotypic 250 μm -thick vibratome slice cultures of 12-13 GW human neocortex tissue. Instead of embedding in a collagen I-based hydrogel, slices were embedded in a poly-(ethylene glycol) (PEG)-based hydrogel. To this end, a 0.07 g/ml PEG diacrylate (PEGDA₇₀₀) solution in DMEM/F12 medium was prepared, which contained 0.1% (wt/vol) 2-hydroxy-2-methylpropiophenone as a photoinitiator to trigger polymerization (see below). This PEG hydrogel was used for two reasons. First, it is not an ECM component and is bio-inert and therefore does not interact with the recombinant HLC proteins added. Second, it has little to no auto-fluorescence. The three ECM components, recombinant HAPLN1, recombinant lumican and native collagen I, were then added to this solution to give the same final concentrations as specified above, 5 $\mu\text{g}/\text{ml}$ each. Control samples (without HLC) received the equivalent volume of PBS to ensure that the final concentration of the hydrogel was the same. The neocortical slices were then transferred to the imaging dishes (Petri dish 35 x 14 mm, including Microwell no.1.5 cover glass (Wong et al., 2014)) and immersed in 100 μl of this hydrogel \pm ECM precursor mix, which was immediately polymerized by exposure to ultraviolet light for five seconds (8000 mW/cm^2 , Delolux 04, Delo GmbH). After polymerization, each dish received 1 ml of SCM.

Two types of live imaging were used, 2-photon imaging and dark-field imaging. For 2-photon imaging, the fluorescent far-red nuclear dye DRAQ5 (5 μM in SCM, eBioscience, 65-0880) was used. This was added to the slices for 30 min prior to the PEG hydrogel embedding, after which the slices were washed in SCM to remove excess DRAQ5, as per manufacturer's guidelines. Slices were then embedded in the PEGDA solution, as described above. Slices were subjected to time-lapse imaging (15-min intervals) using a Leica DMI6000 inverted 2-photon microscope using a Leica HC CS PL APO 10x 0.4 objective. For dark-field time-lapse imaging (15-min intervals), slices (not subjected to DRAQ5 labeling) were imaged using a Zeiss Axiovert 200M inverted microscope using a Zeiss Plan-Neofluar 5x 0.15 Ph1 objective. For both types of live imaging, slice cultures were maintained at 37°C in the presence of humidified 40% O₂ / 5% CO₂ / 55% N₂, as above. Imaging was started 2-4 h after the embedding of slice cultures.

ECM component selection

The three ECM components HAPLN1, lumican and collagen I were identified by screening of several existing transcriptome datasets. ECM components were identified from the core matrisome published by the matrisome project (Naba et al., 2012), resulting in a total of 288 genes. In the datasets (Fietz et al., 2012; Florio et al., 2015), we screened for ECM components whose mRNAs were more highly expressed in human neocortical progenitor cell types or germinal zones in comparison to mouse, resulting in a total of 196 genes. Once this list of ECM components was generated, it was compared to another dataset from E9.5 mouse neuroepithelium (Albert et al., 2017), from which we generated a list of ECM components that were expressed at this early stage, but the expression of which was decreased or lost at E14.5 in mouse neocortex (Fietz et al., 2012; Florio et al., 2015), resulting in 58 genes. This was done to identify ECM components that were expressed in human neocortex and specifically down-regulated in the mouse developing neocortex, as these were candidates likely to have an evolutionary role in neocortex development. Of these 58 genes, were excluded those with a FPKM value of less than 2, to identify ECM components with a mid-high level of expression. This resulted in 28 genes. From these 28, we next selected genes with a FPKM value of less than 1 in mouse NPCs, to identify ECM components with lowest expression in the mouse at the peak of neurogenesis. This resulted in a total of 9 genes (Table S1). Finally, we selected those genes with the highest expression in the human, with a FPKM value over 4. This comparison identified the 3 ECM components selected: HAPLN1, lumican and collagen I (from the subunit Col1a2).

QUANTIFICATION AND STATISTICAL ANALYSIS

All image analyses and quantifications were conducted using Fiji, and all statistical analyses were conducted using GraphPad Prism. All datasets were tested for Gaussian distribution (Kolmogorov-Smirnov test) prior to the selection of the appropriate statistical test; Students' *t*-test, one-way ANOVA or two-way ANOVA (details of statistics used can be found in the figure legends). All datasets were analyzed blind.

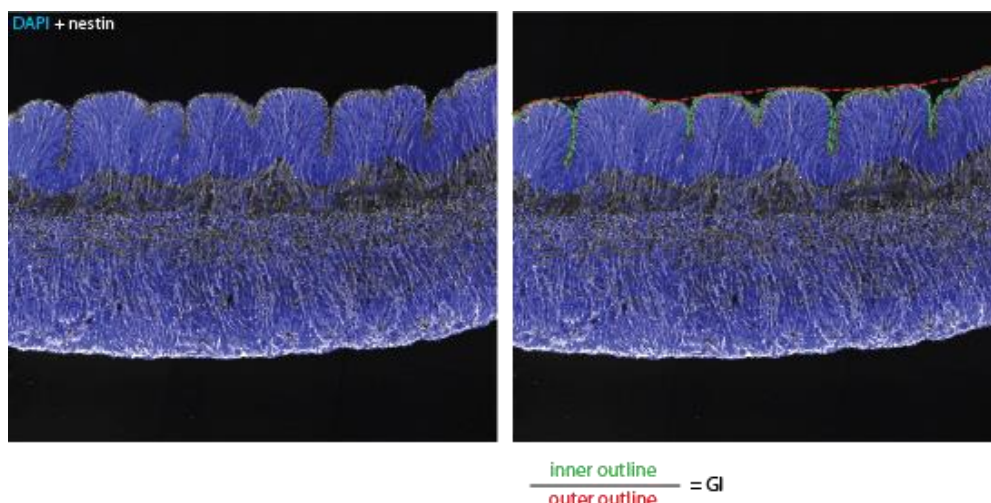
For quantification of IF, Fiji was used to measure the pixel density of HA, pERK1/2, p90RSK and His-tag staining. Measurements were taken within a defined region of interest (ROI) (100 μ m x 100 μ m) in the VZ and CP (HA), or just within the CP (pERK1/2 and p90RSK), or within the VZ, SVZ, IZ and CP (His-tag) of each cryosection. For one human fetal or ferret embryonic sample, a minimum of 3 ROIs were measured per zone within a

single cryosection, and a minimum of 3 cryosections were analyzed per sample, followed by calculation of the average pixel density in each zone and sample.

To allow the quantification of HA levels across human fetal samples of different developmental stages, different handling (Dresden vs. HDBR), and given that the exact location of tissue pieces within the neocortex was unknown, the HA IF in the CP was expressed relative to that in the VZ in each sample. For pERK1/2 and p90RSK IF, the averaged pixel density was compared to control values for each experiment, and therefore the data are presented relative to control (control values were set to 1.0). For HA and pERK quantifications, 5 individual human fetal samples were used of ages ranging from 11-14 GW, for p90RSK 3 individual human fetal samples were used of ages ranging from 13-14 GW. For His-tag quantification, the averaged pixel density in control was taken as background. This value was then subtracted from the pixel density measurements for HLC-/HAPLN1 alone-/lumican alone-treated tissue.

Nuclear distance measurements were taken in a defined ROI (30 μm x 40 μm). From each cryosection, 3-6 ROIs were measured within the CP and (if applicable) in the gyrus and sulcus. For each ROI, 4 optical sections within a 3- μm z-depth range, compressed into a single image, were used for measurements. To measure the distance between nuclei, 10-15 nuclei per ROI were randomly selected. The distances between the outer surface of the nucleus to all neighboring nuclei were then measured. For each condition, 300-400 distances were measured in 3 individual fetuses.

Quantification of the gyrification index was determined in a similar manner to in vivo measurements (Zilles et al., 1988) (see images below).



DATA AND SOFTWARE AVAILABILITY

RNA-seq raw data have been deposited with the Gene Expression Omnibus under accession codes GSE106640.

Abbreviations

AFM	Atomic force microscopy
ChondABC	Chondroitinase ABC
CP	Cortical plate
DS	Down syndrome
E	Embryonic day
ECM	Extracellular Matrix
Exp.	Experiment
FFTC	Free floating tissue culture
GI	Gyrification index
GW	Gestation week
h	hours
HA	Hyaluronic acid
HAS	Hyaluronic acid synthase
HLC	HAPLN1, lumican and collagen I
HuNcx	Human neocortex
Hyal	Hyaluronidase
Ind. exp.	Independent experiment
NDDs	Neurodevelopmental disorders
NPC	Neural progenitor cell
P	Postnatal day
PME	Prenatal methamphetamine exposure

Supplemental Materials

Fig S1 – S8

Movies S1 - S3

Tables S1 - 2

Movie legends

Movie S1. Human neocortex organotypic slice culture, control, imaged for 24 h. Related to Figure 2.

Organotypic slice culture of 12 GW human neocortex. Tissue has been stained with far red nuclei dye, DRAQ5, and embedded in PEG hydrogel. Images were taken every 15 min for 24 h. The CP (top of the image) remains unfolded throughout imaging. Time lapse imaging was performed using a 2-photon confocal and 10x magnification.

Movie S2. Human neocortex organotypic slice culture, with HLC-treatment, imaged for 24 h. Related to Figure 2.

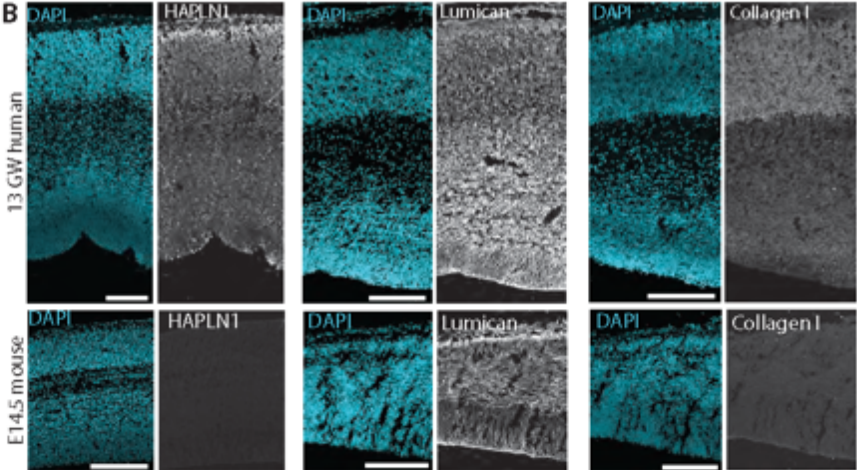
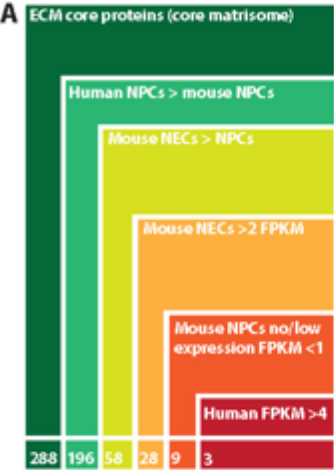
Organotypic slice culture of 12 GW human neocortex. Tissue has been stained with far red nuclei dye, DRAQ5, and embedded in PEG hydrogel. Images were taken every 15 min for 24 h. The CP starts to fold after 6 h, continues folding for the next 12 h before becoming stable for the last few hours of imaging. Time lapse imaging was performed using a 2-photon confocal and 10x magnification.

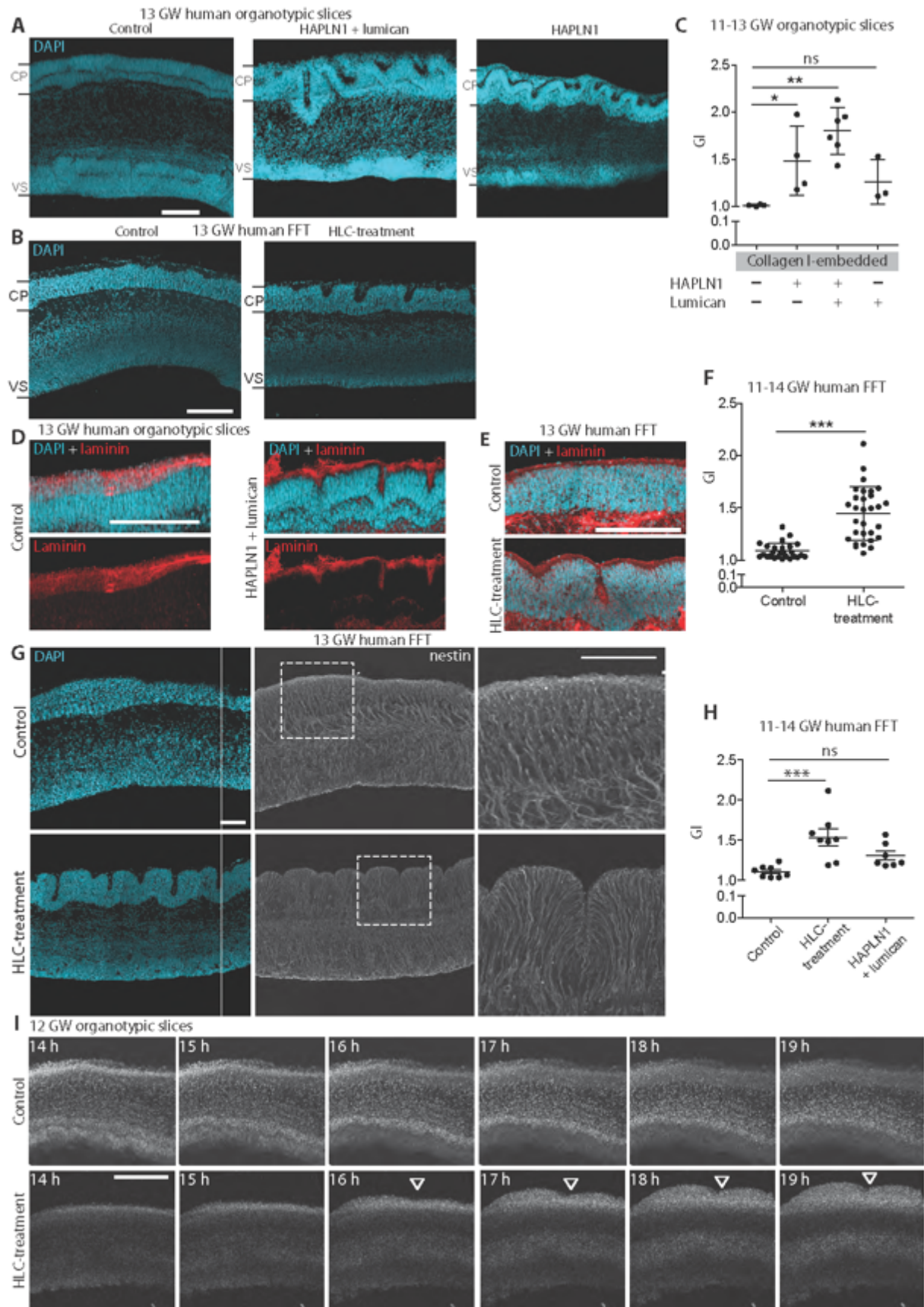
Movie S3. Human neocortex organotypic slice culture, HLC-treated with the addition of hyaluronidases after 24 h, imaged for 72 h. Related to Figure 4.

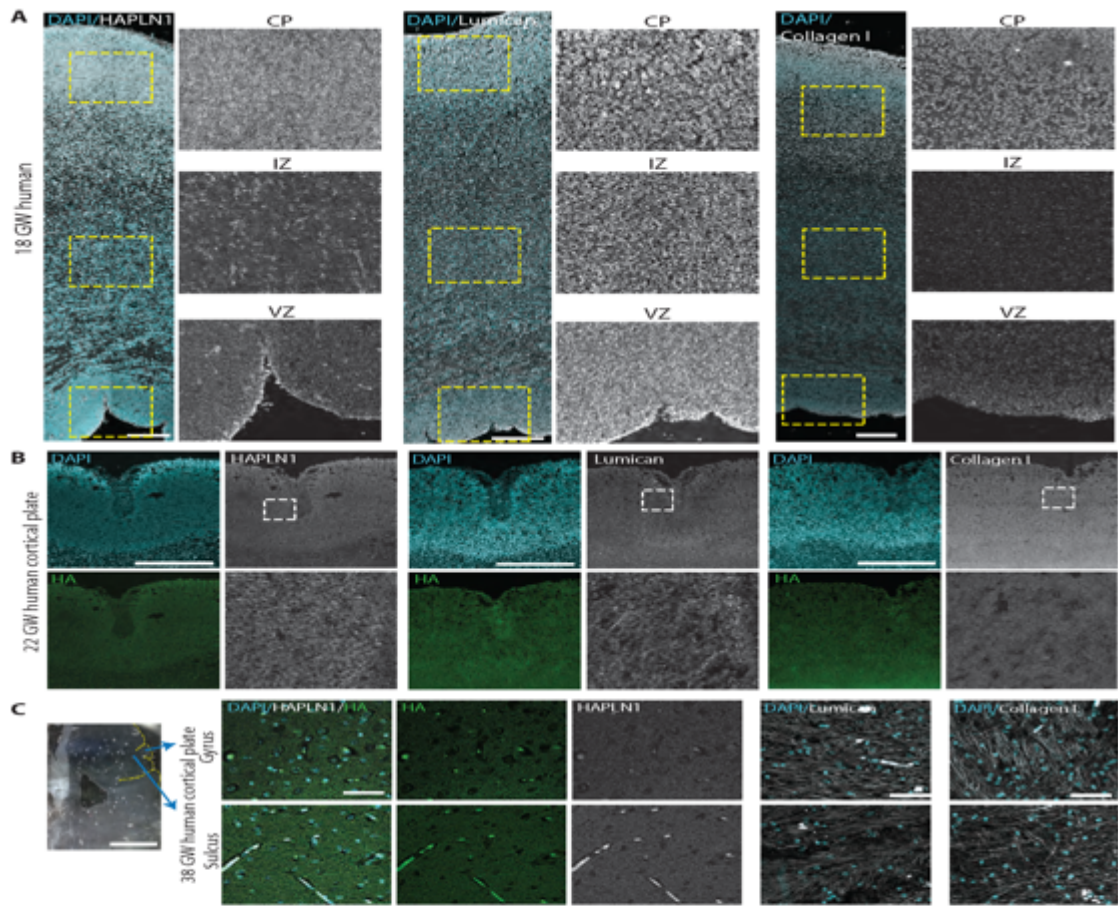
Organotypic slice culture of 13 GW human neocortex. Tissue was imaged on a wide-field system, using dark-field imaging, so did not require staining. Images were taken every 15 min for 72 h. Imaging started 4 h after the addition of HLC, folding is already starting to occur. The CP continues to fold for the next 20 h. Hyaluronidases were then added to the slice culture (when indicated by label). The CP then unfolds, returning to the original smoothness and size over the next 48 h. Time-lapse imaging was performed using a wide-field system and 5x magnification.

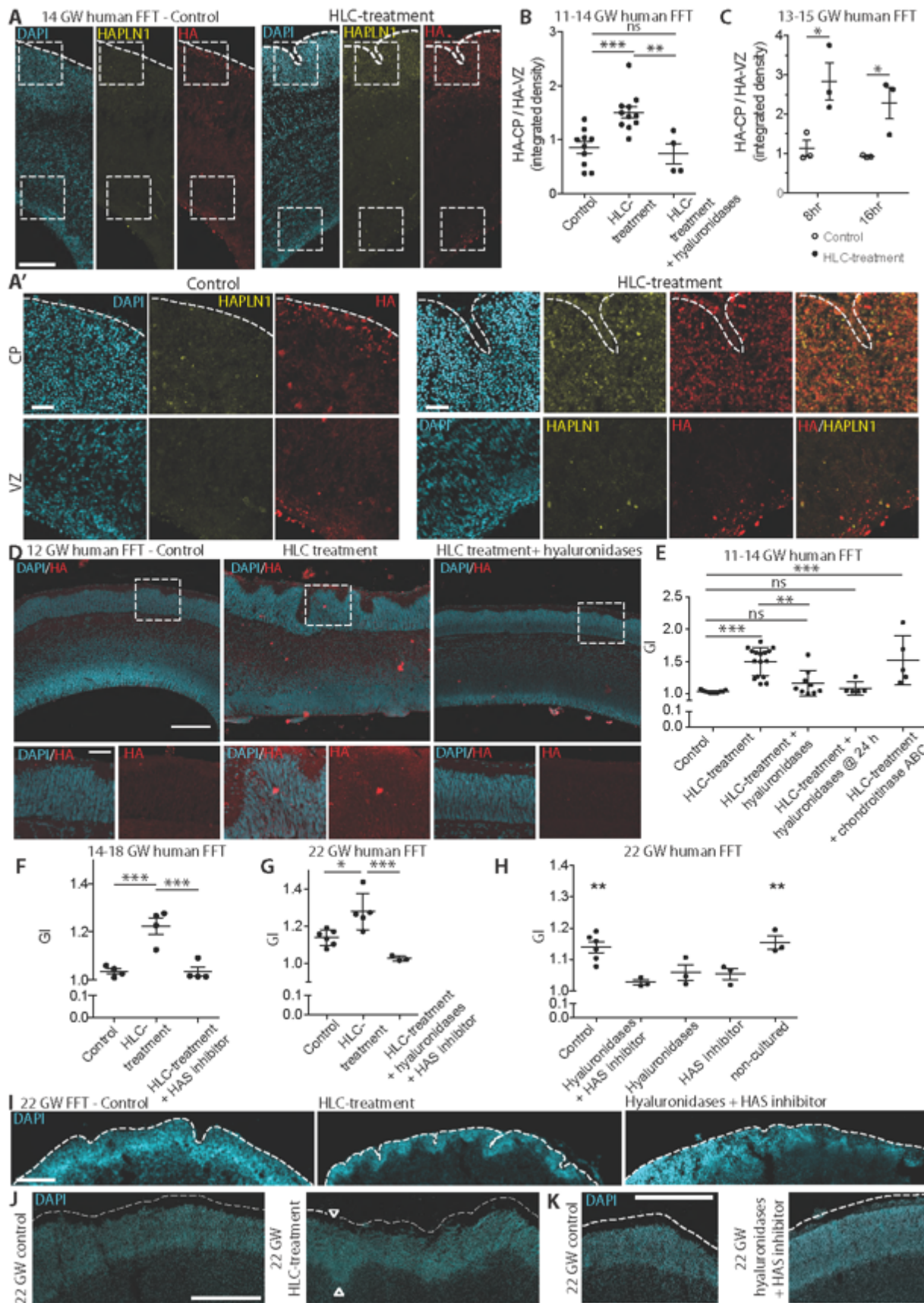
Supplemental Excel table S1.

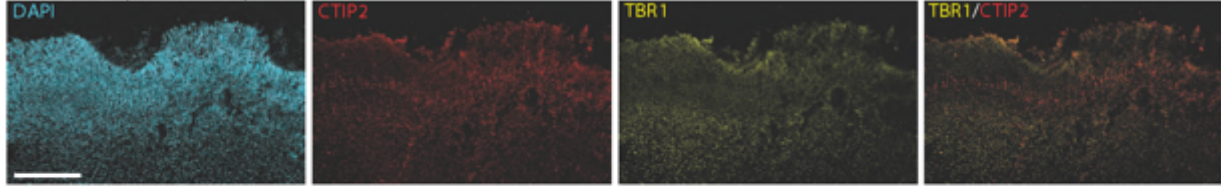
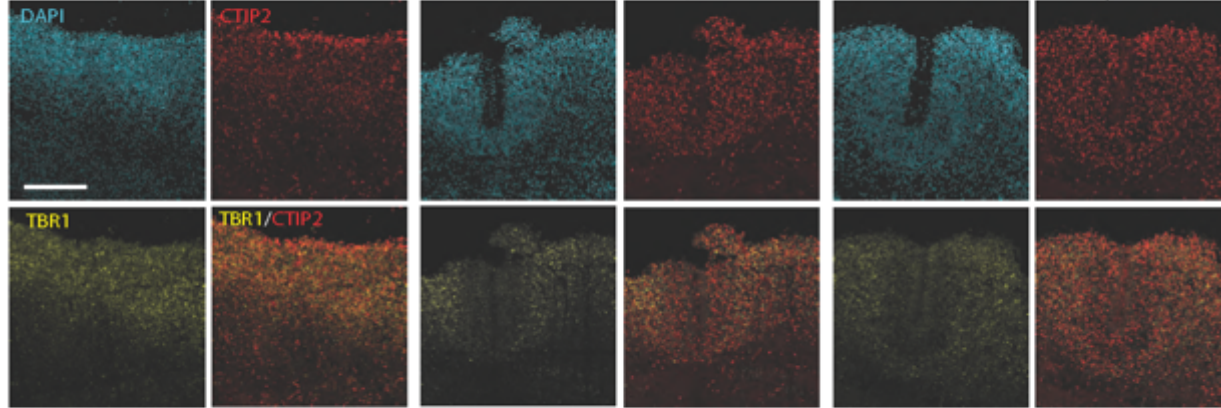
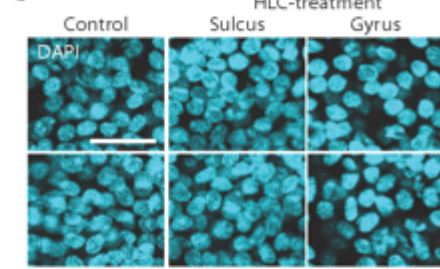
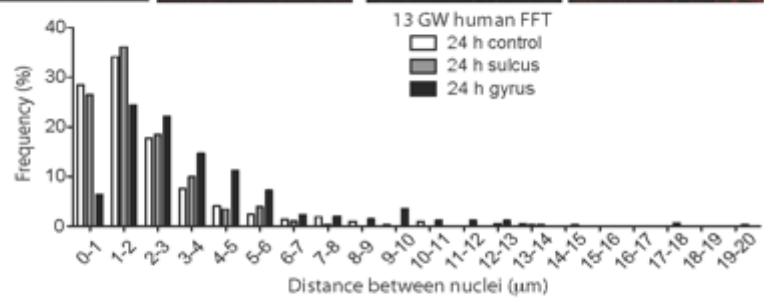
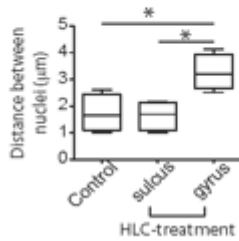
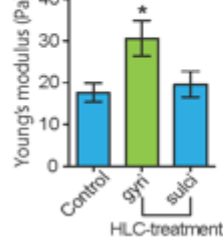
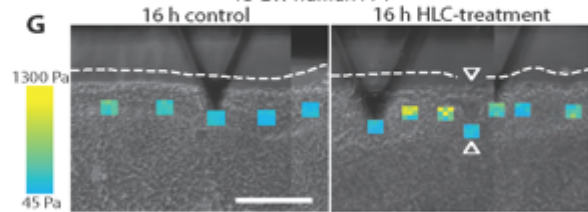
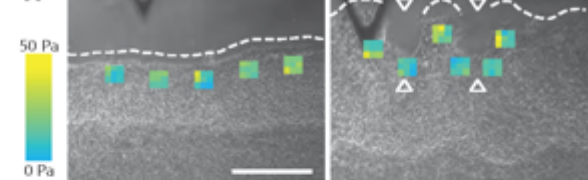
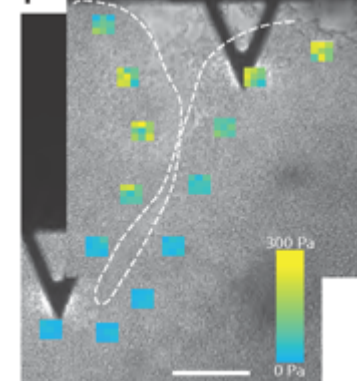
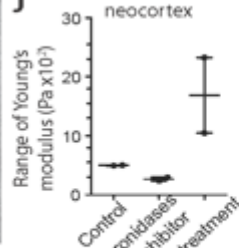
Table S1. Gene enrichment lists from RNAseq. Related to Figure S6D and **Figure 4.**

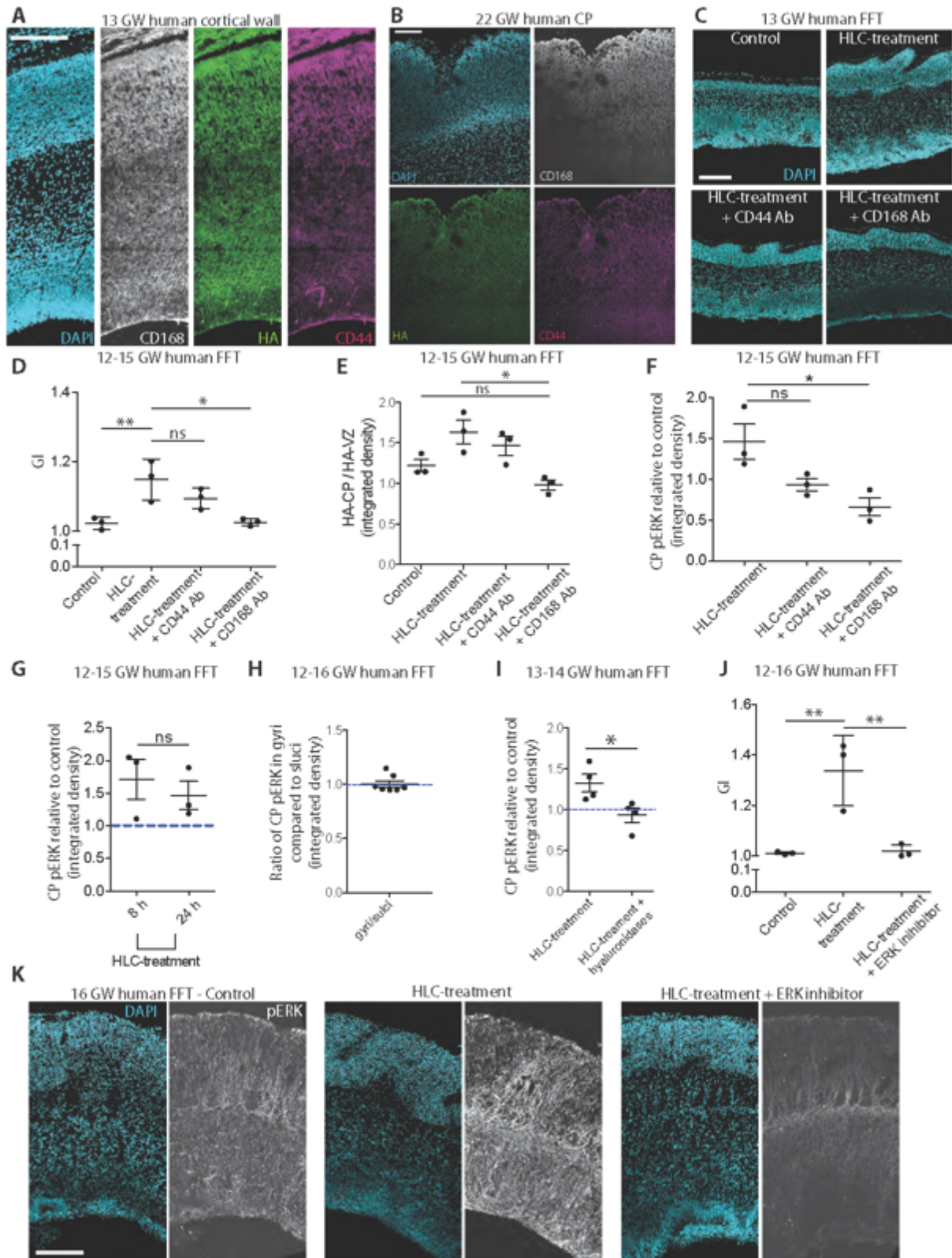


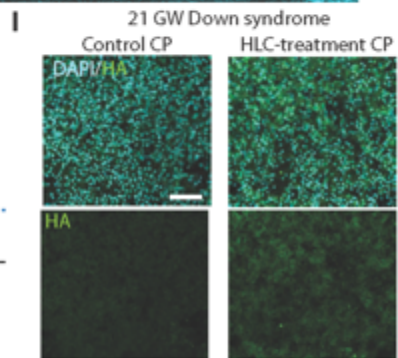
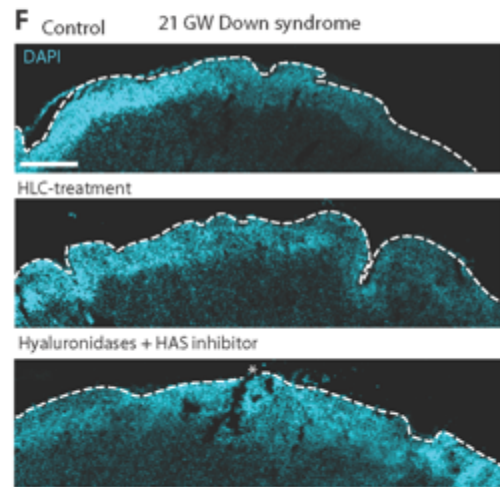
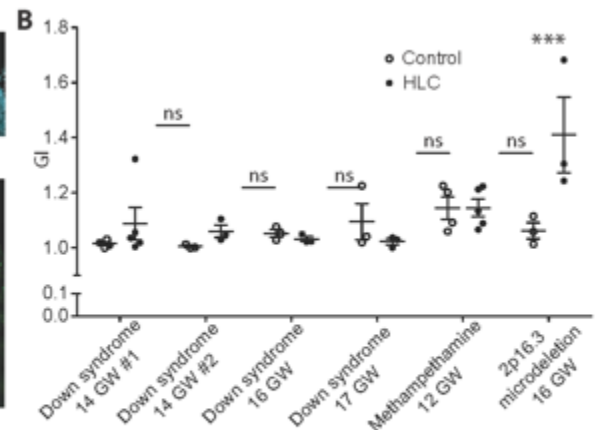
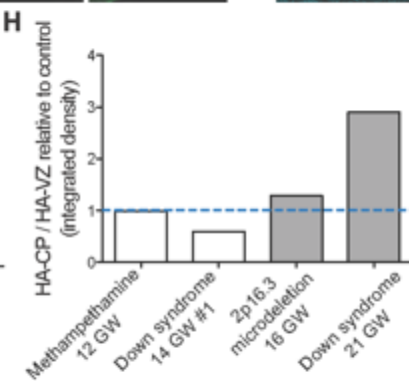
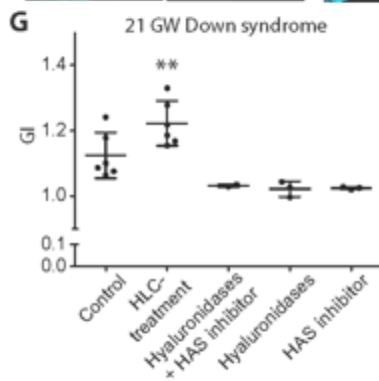
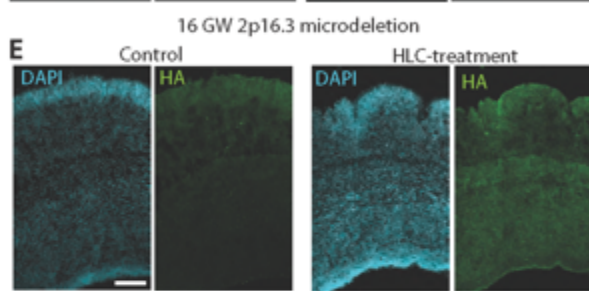
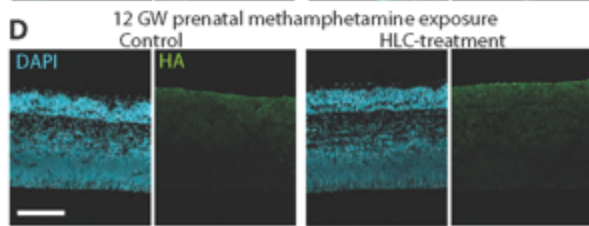
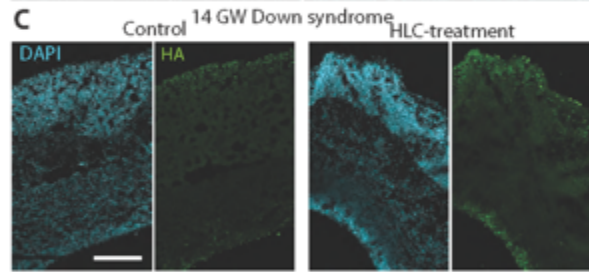
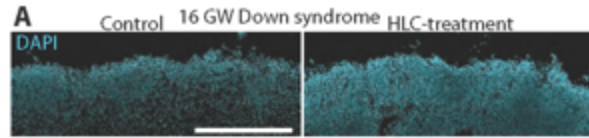






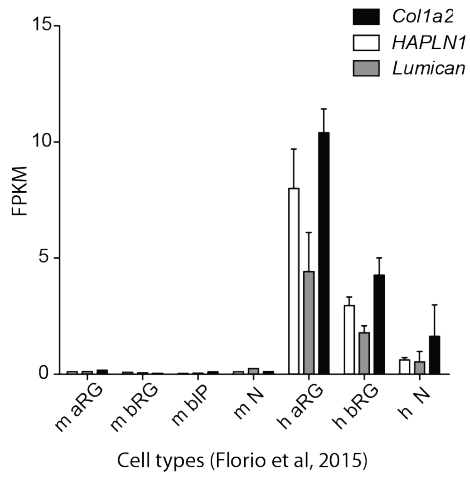
A 22 GW CP (non-cultured)**B** 15 GW human FFT - Control**C** 13 GW human FFT**D****E** 13 GW human FFT**F** 12-14 GW human FFT**G** 13 GW human FFT**H** 24 h control**I** 22 GW non-cultured neocortex**J** 22 GW non-cultured neocortex



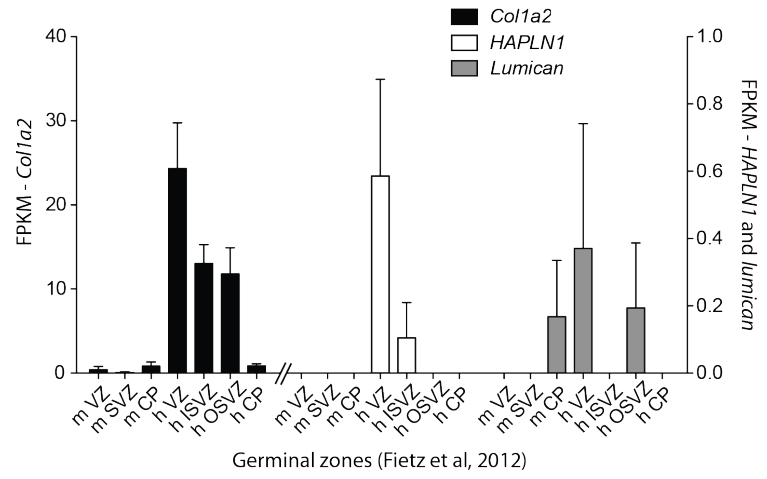


Supplemental figures

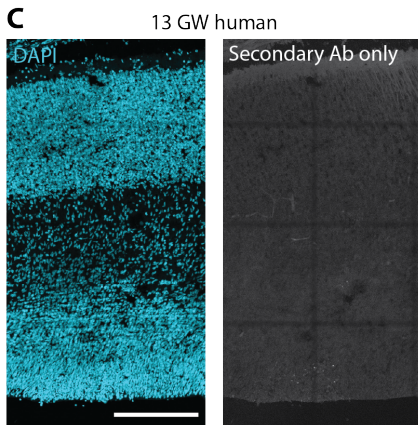
A



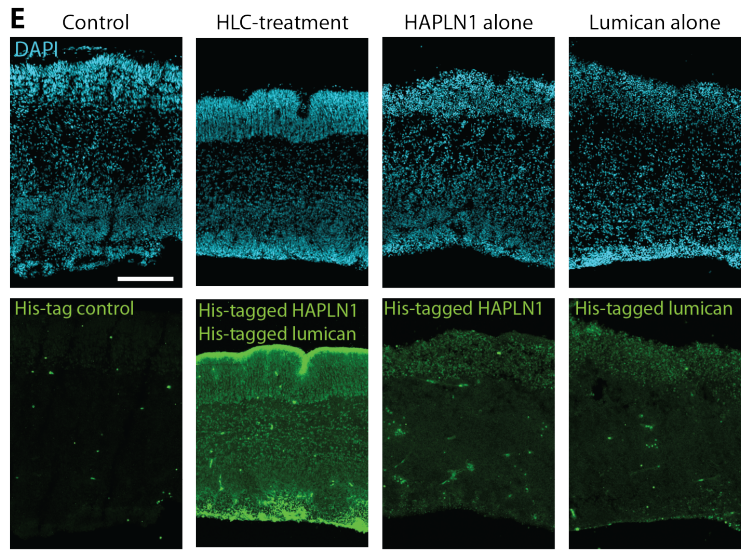
B



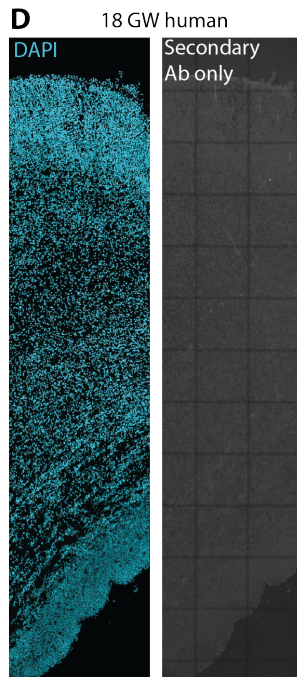
C



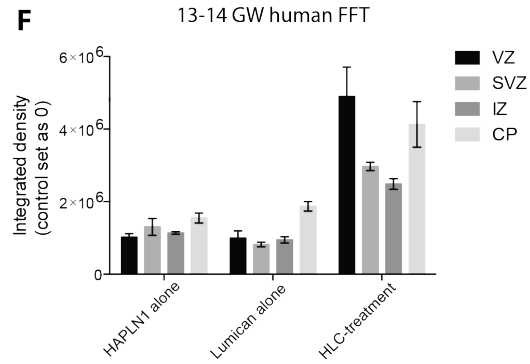
E



D



F



Supplemental Figure 1. *HAPLN1*, *lumican* and *colla2* mRNA expression in embryonic mouse and fetal huNcx, secondary antibody control for IF of HAPLN1, lumican and collagen I, and His-tag IF of recombinant proteins in huNcx. Related to Figures 1-2.

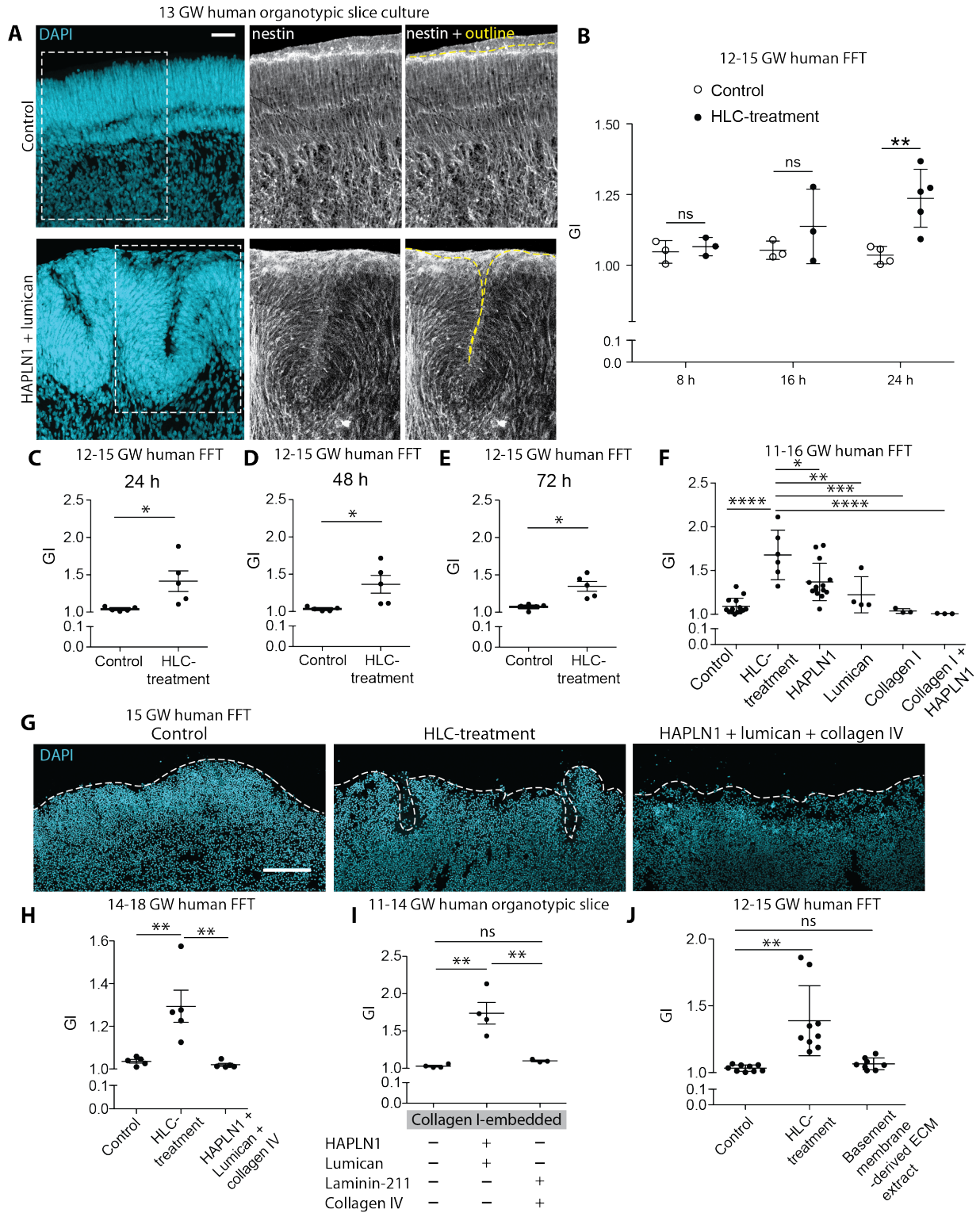
mRNA expression data are taken from Florio et al, 2015 (16) (A) and Fietz et al, 2012 (21) (B) transcriptome datasets. *Colla2* is a subunit of collagen I. (A) FPKM values for cell populations isolated from embryonic mouse (m) and fetal human (h) neocortex. aRG, apical radial glia; bRG, basal radial glia; bIP, basal intermediate progenitor-enriched fraction; N, neuron fraction (note that the human neuron fraction contains not only neurons but also basal radial glia in G1 (16), which likely account for the low levels of *HAPLN1*, *lumican* and *Colla2* mRNA expression observed in this fraction). (B) FPKM values for specific zones of embryonic mouse (m) and fetal human (h) neocortex. The FPKM values for *Colla2* are shown on the left y-axis, the *HAPLN1* and *lumican* FPKM values are shown on the right y-axis, as indicated by the break in the x-axis. VZ, ventricular zone; SVZ, subventricular zone; CP, cortical plate; ISVZ, inner SVZ; OSVZ, outer SVZ. (A, B) Error bars, SD.

(C, D) DAPI staining (blue) and rabbit-647 secondary antibody IF (grey) of 13 GW (a) and 18 GW (b) huNcx. This rabbit-647 secondary antibody is a control for all HAPLN1, lumican and collagen I IF (Figure 3), as all primary antibodies were raised in rabbit.

(E) DAPI staining (blue) and His-tag IF (green, used to detect the His-tagged recombinant HAPLN1 and lumican added) of 13 GW huNcx in FFTC subjected to control, HLC-treatment, HAPLN1 alone and lumican alone for 24 h.

(F) Quantification of His-tag pixel density measured in the VZ, SVZ, IZ and CP for the indicated treatments. Error bars, SEM.

(C, D, E) Scale bars: 200 μ m.



Supplemental Figure 2. 13 GW huNcx slice cultures and analysis of the effect of other ECM components and time points on HLC-induced folding. Related to Figure 2.

(A) DAPI staining (blue) and nestin IF (grey) of CP of 13 GW huNcx. Dashed boxes delineate panels to the right. Yellow dashed lines outline the smooth (top) and folded (bottom) CP.

(B) Quantification of GI of 12-15 GW huNcx subjected to control and HLC-treatment in FFTC for 8, 16 and 24 h, *, $P=0.004$ (B), 24 h, *, $P=0.0273$ (C), 48 h, *, $P=0.024$ (D) and 72 h **, $P=0.0038$ (E).

(F) Quantification of GI in 11-16 GW huNcx in FFTC subjected to the indicated conditions for 24 h. ****, control vs. HLC-treatment $P<0.0001$, collagen I + HAPLN1 vs. HLC-treatment $P<0.0001$; ***, $P=0.0001$; **, $P=0.0042$, *, $P=0.0137$. Not shown: control vs. HAPLN1, *, $P=0.0023$; control vs. all other conditions, ns, $P>0.05$.

(G) DAPI staining of 15 GW huNcx in FFTC subjected to control (left), HLC-treatment (middle) and HAPLN1 + lumican + collagen IV treatment (right). White dashed lines outline the unfolded (left and right) or folded (middle) CP surface.

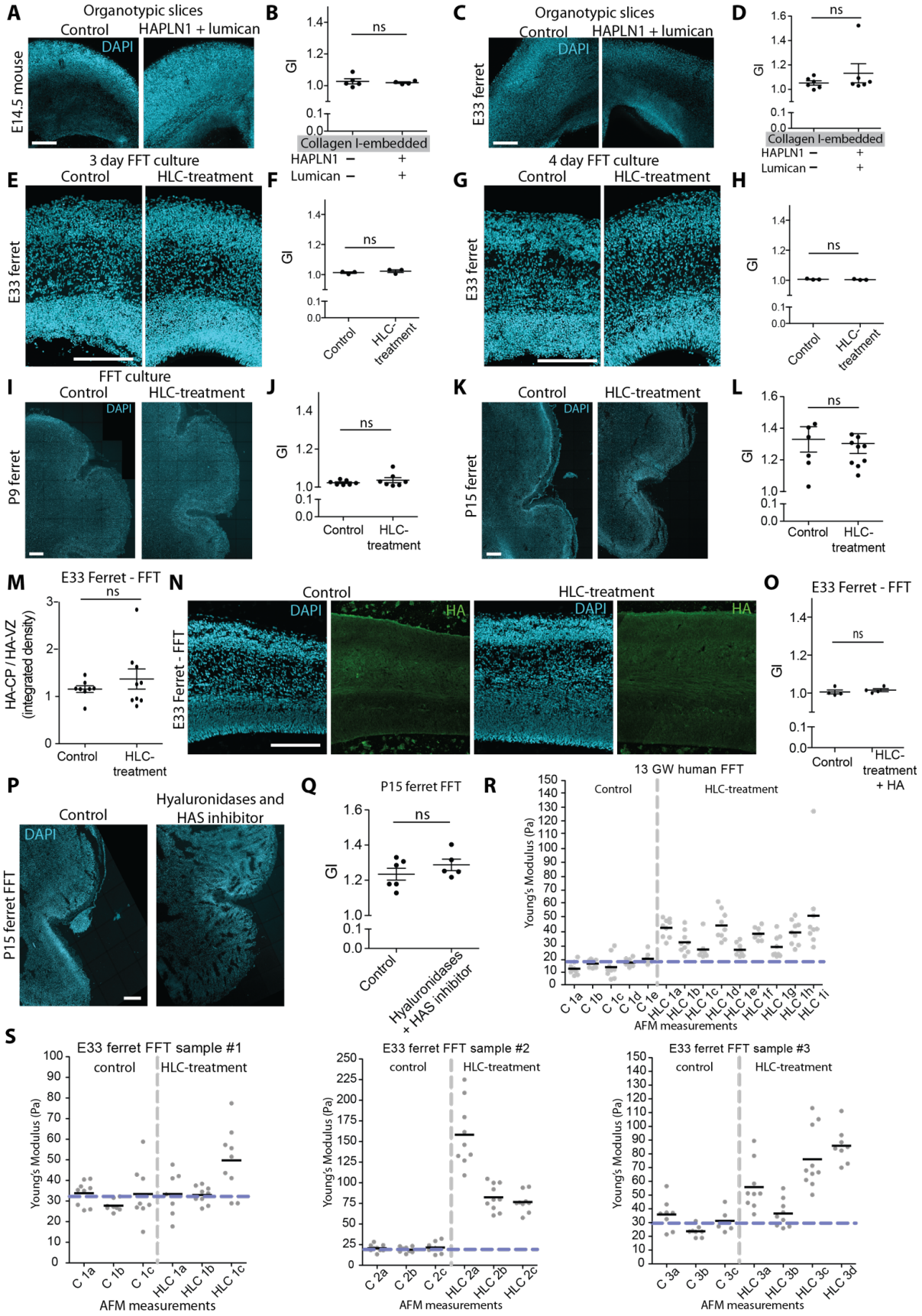
(H) Quantification of GI of collagen I-embedded 11-14 GW huNcx in organotypic slice culture subjected to the indicated conditions. **, $P=0.0013$ (control vs. HLC-treatment), $P=0.0041$ (HLC-treatment vs. Laminin-211 + collagen IV).

(I) Quantification of GI in 14-18 GW huNcx in FFTC subjected to the indicated conditions. **, $P=0.0035$ (control vs. HLC-treatment), $P=0.0022$ (HLC-treatment vs. HAPLN1 + lumican + collagen IV).

(J) Quantification of GI in 12-15 GW huNcx in FFTC subjected to control, HLC-treatment and treatment with a basement membrane-derived ECM extract. ***, $P=0.0002$ (control vs. HLC-treatment), $P=0.0009$ (HLC-treatment vs. HLC-treatment + basement membrane-derived ECM extract).

Scale bars: (G) 200 μm .

(B-F, H-J) Statistical tests; two-way ANOVA (B), Student's *t*-test (C-E), one-way ANOVA (F, H-J). Error bars, SD; ns, $P>0.05$. Data points represent 3 ind. exp. (1 fetus/exp.) with 1-2 FFTCs per condition per fetus and fetal samples in (B) are independent of fetal samples in (C-E), in (F, H-J) represent 3-5 ind. exp. (1 fetus/exp.) with 1-3 slice cultures or FFTCs per condition per fetus.



Supplemental Figure 3. HLC-treatment does not induce folding of developing mouse and ferret neocortex and loss of HA does not perturb folding of developing ferret neocortex.

Related to Figure 5.

(**A, C, E, G, I, K**) DAPI staining of collagen I-embedded E14.5 mouse neocortex (**A**) and E33 ferret neocortex (**C**) in organotypic slice culture subjected to control (left) and HAPLN1 plus lumican treatment (right) for 24 h, and of E33 ferret neocortex in FFTC subjected to control (left) and HLC-treatment (right) for 3 (**E**) and 4 days (**G**), and P9 (**I**) and P15 (**K**) ferret neocortex in FFTC for 2 days.

(**B, D, F, H, J, L**) Quantification of GI of developing mouse and ferret neocortex subjected to the culture conditions and treatments specified in (**A, C, E, G, I, K**), respectively.

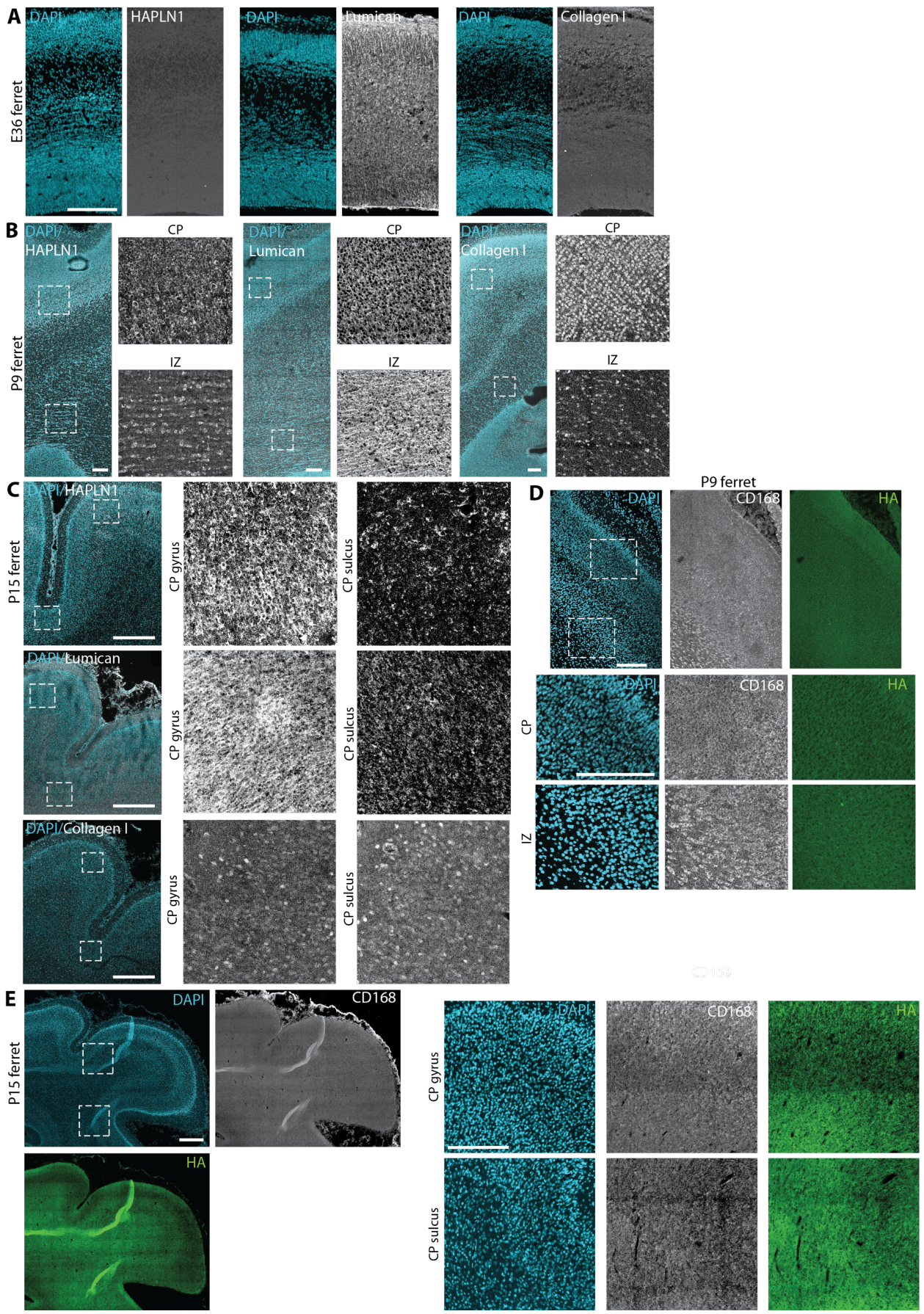
(**M-O**) E33 ferret neocortex in FFTC subjected to control and either HLC-treatment (**M, N**) or HLC-treatment with addition of HA (**O**), for 24 h. (**M**) Quantification of the CP/VZ ratio of HA immunoreactivity. (**N**) DAPI staining (blue) and HA IF (green). (**O**) Quantification of GI of E33 ferret neocortex subjected to the indicated treatments for 48 h.

(**P, Q**) P15 ferret neocortex in FFTC subjected to control and treatment with hyals plus HAS inhibitor for 48 h. (**P**) DAPI staining (blue). (**Q**) Quantification of GI. Statistical test used; Student's *t*-test. Error bars, SD; ns, $P > 0.05$. Data points represent 3 ind. exp. (1 P15 ferret/exp.) with 1-2 FFTCs per condition per ferret. Note the lack of sensitivity of the developing ferret neocortex folding to the reduction of HA levels.

(**R, S**) AFM values of consecutive regions (indicated by small letters) of the same respective cryosection from 13 GW huNcx (**R**) and E33 ferret neocortex (three embryos from one litter) (**S**) in FFTC subjected to control (C) and HLC-treatment (HLC) for 24 h. Blue dashed lines indicate the average of the control values of the respective cryosection, grey dashed lines separate the control and HLC values.

(**A, C, E, G, I, K, N, P**) Scale bars: 200 μm .

(**B, D, F, H, J, L, M, O, Q**) Statistical test used; Student's *t*-test. Error bars, SD; ns, $P > 0.05$. Individual data points in (**B, D, F, H, J, L, M, O**) represent the average value from an individual embryo (average of 3 images per embryo), from E14.5 mouse or E33, P9 and P15 ferret, from 3 independent litters, and in (**Q**) 3 ind. exp. (1 P15 kit/exp.) with 1-2 FFTCs per condition per kit.

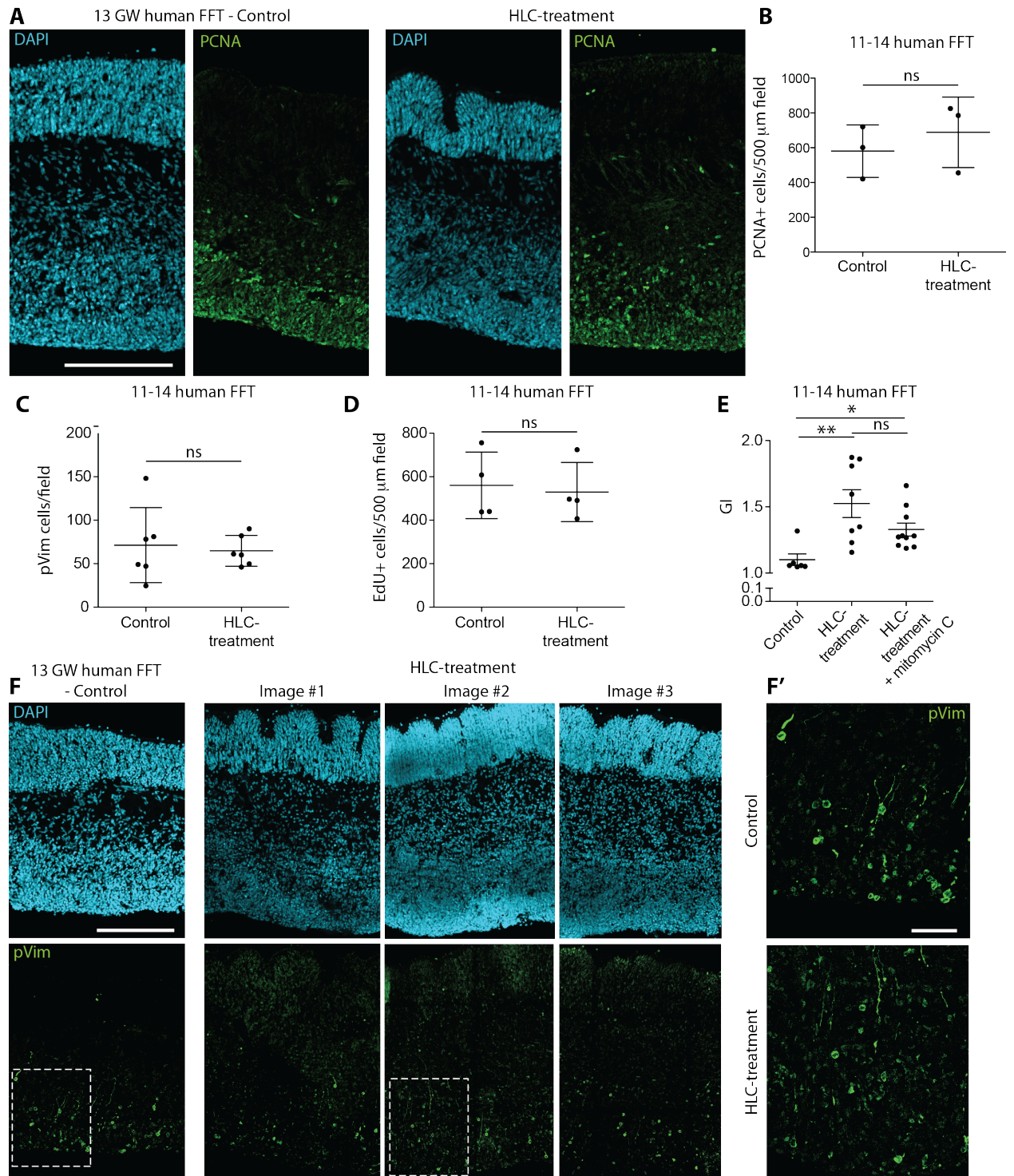


Supplemental Figure 4. HAPLN1, lumican, collagen I, CD168 and HA IF in developing ferret neocortex. Related to Figure 3.

(A-C) DAPI staining (blue) and either HAPLN1, lumican, collagen 1 IF (grey, as indicated) of E36 (A), P9 (B) and P15 (C) developing ferret neocortex. Dashed boxes in (B) delineate the P9 CP and IZ areas shown in (top and bottom row, respectively), and in (C) the P15 CP gyrus and sulcus areas shown in (left and right panels, respectively).

(D, E) DAPI staining (blue) and double IF for CD168 (grey) and HA (green) of P9 (D) and P15 (E) developing ferret neocortex. Dashed boxes in (D) delineate the P9 CP and IZ areas shown in (top and bottom row, respectively), and in (E) the P15 CP gyrus and sulcus areas shown in (top and bottom row, respectively).

Scale bars: (A-D) 200 μm and (E) 500 μm .



Supplemental Figure 5. HLC-treatment does not cause an overt increase in cycling cortical progenitor cells, and cell proliferation is not essential for the HLC-induced GI increase.

Related to Figure 6.

(A) DAPI staining (blue), and PCNA IF (green) of 13 GW huNcx in FFTC subjected to control (left 2 panels) and HLC-treatment (right 2 panels).

(B-D) Quantification of the total number of (B) PCNA-positive cells per 500 μm wide area, (C) pVim-positive cells per microscopic field (2000 μm wide area of tiled-images and (D) EdU-positive cells per 500 μm wide area, EdU was given 1 hour prior to fixation, in 11-14 GW huNcx in FFTCs subjected to control and HLC-treatment for 24 h.

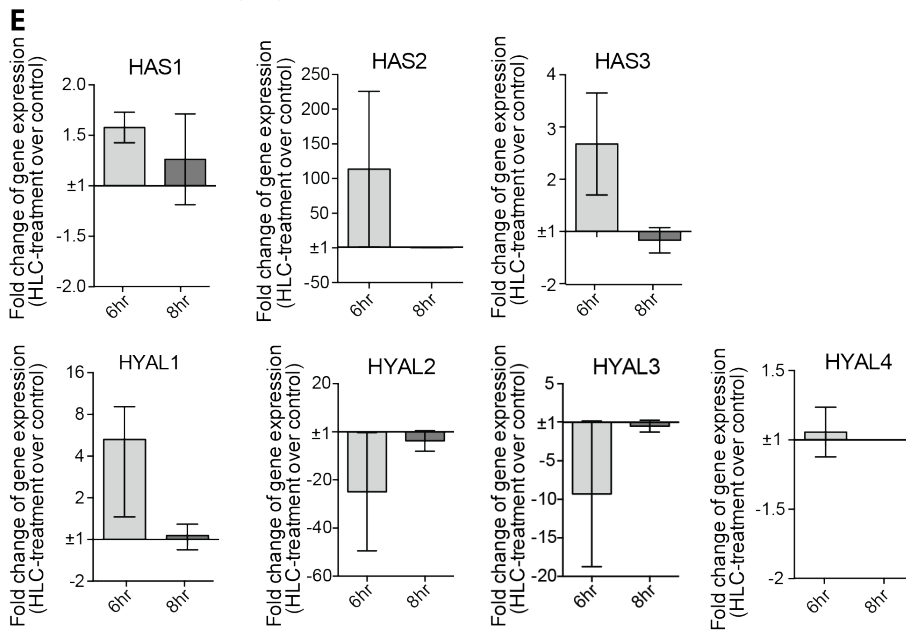
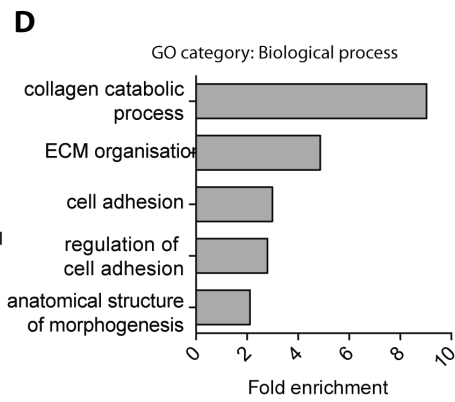
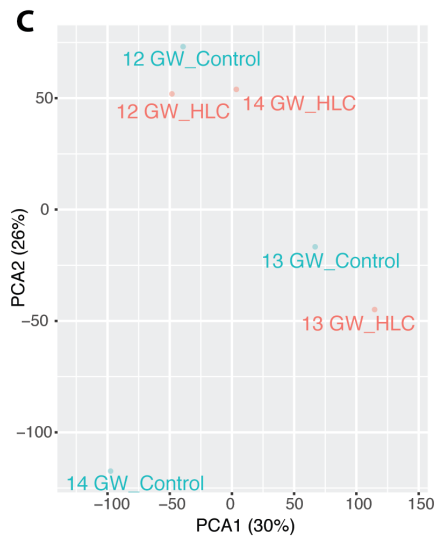
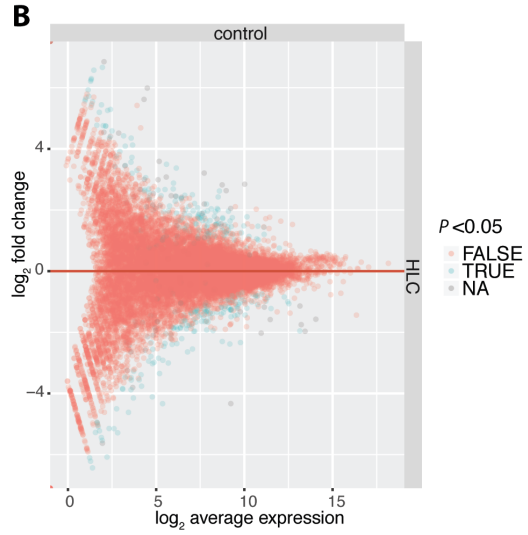
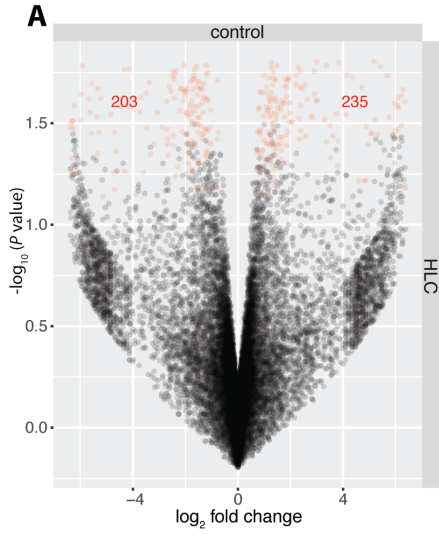
(E) Quantification of GI of 11-14 GW huNcx in FFTC subjected to control, HLC-treatment and HLC-treatment with the addition of the inhibitor of proliferation, mitomycin C (10 $\mu\text{g}/\text{ml}$), for 24 h. *, $P=0.0489$; ***, $P=0.0009$.

(F) DAPI staining (blue, top row), and IF for the mitotic marker phospho-vimentin (pVim, green, bottom row) of 13 GW huNcx in FFTC subjected to control (left) and HLC-treatment (3 examples are shown, 3 right panels) for 24 h. Dashed boxes delineate the areas of pVim IF in (A').

Note that the cell cycle length of human neocortical progenitors is estimated to be substantially greater than 24 h (Hansen et al., 2010, Betizeau et al., 2013, LaMonica et al., 2013).

(A, F, F') Scale bars: (A, F) 200 μm and (F') 50 μm .

(B-E) Statistical test used; Students' t -test (B-D), one-way ANOVA (E). Error bars, SD; ns, $P > 0.05$. Data points represent 3 ind. exp. (1 fetus/exp.) with 1-3 FFTCs per condition per fetus.



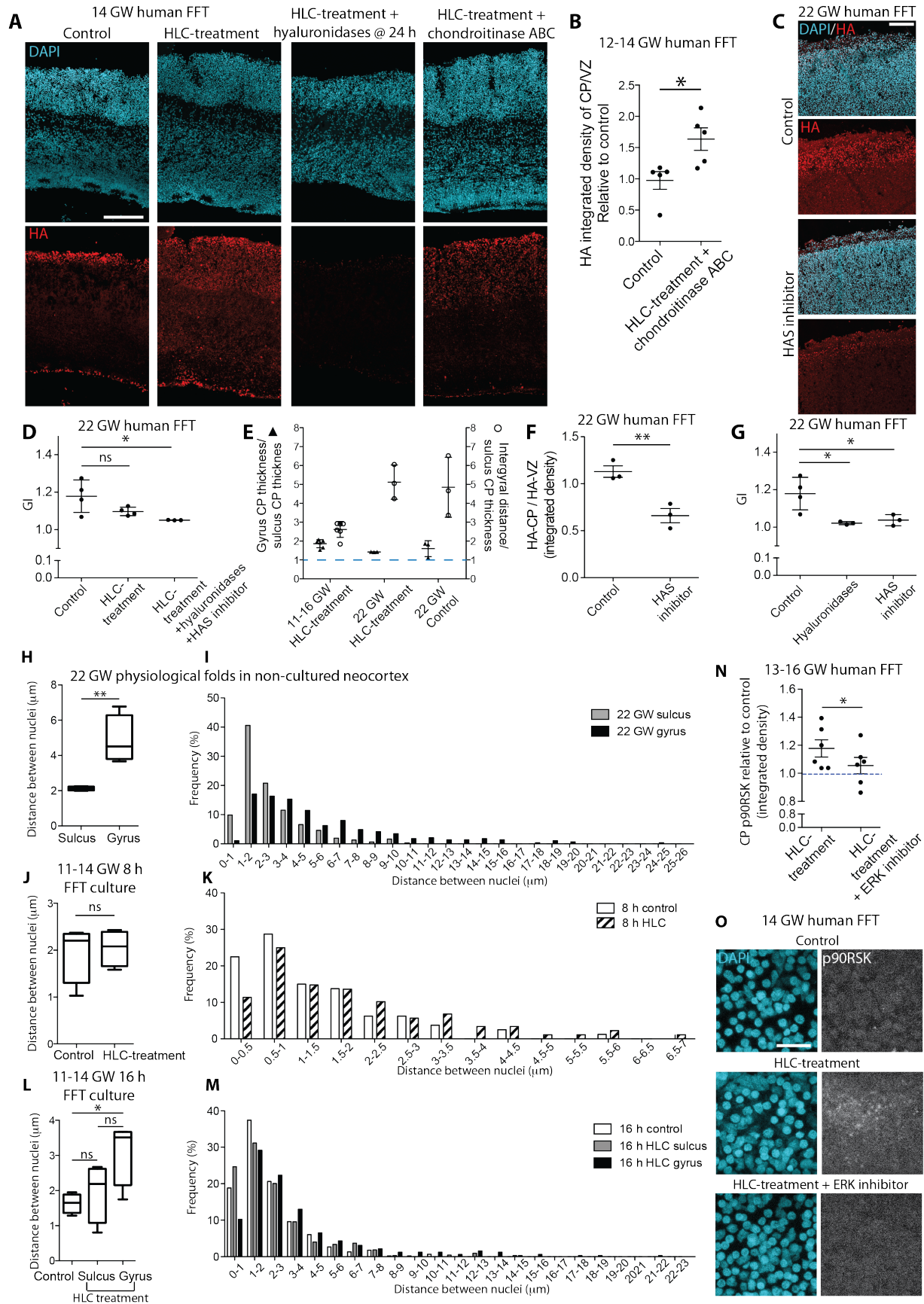
Supplemental Figure 6. RNA sequencing of HLC-treated and control CP and qPCR analysis of HAS1-3 and HYAL1-4 in huNcx in FFTC for 6 and 8 h. Related to Figure 4.

Laser capture microdissection (LCM) was used to isolate the CP from 12-14 GW huNcx in control and HLC-treatment (HLC) for 16 h of FFTC (when folding has just started). When HLC-treated CP was compared to control CP using the standard cut-off levels of significance ($P < 0.01$), zero differentially expressed genes were identified. When this cut-off level was raised to $P < 0.05$, a total of 235 genes were found to be up-regulated after HLC-treatment and 203 were down-regulated, as shown in the volcano plot (A) of differentially expressed genes ($P < 0.05$). True and False indicate if the differential expression of the gene is statistically significant. (B) MA plot of differentially expressed genes ($p < 0.05$) of HLC-treatment CP compared to control. True and False indicate if the differential expression of the gene is statistically significant, NA indicates not applicable.

(C) Principle component analysis (PCA) plot of the 3 HLC-treated samples (red) and control (blue) samples.

(D) Fold enrichment of GO biological process terms from RNAseq analysis. Terms listed all show a fold enrichment greater than 2 and have a $P < 0.05$. The genes included within these terms are outlined in table S2.

(E) qPCR analysis of mRNA levels of *HAS1-3* and *HYAL1-4* in 13-16 GW huNcx in FFTC subjected to control and HLC-treatment for 6 and 8 h. Data is represented as fold change in HLC-treatment compared to control. Three independent qPCR experiments were performed (1 fetus/exp.). Error bars, SEM.



Supplemental Figure 7. 24-hour HLC-treatment and degradation of HA in 22 GW huNcx, analysis of HA levels after HLC-treatment + hyals or chondABC in 12-14 GW huNcx, analysis of the distance between nuclei in the CP of 11-14 GW huNcx in FFTC and of non-cultured 22 GW huNcx, and analysis of p90RSK. Related to Figures 4-6.

(A) DAPI staining (blue) and IF for HA (red) in 14 GW huNcx in FFTC subjected to control (far-left), HLC-treatment (centre left), HLC-treatment + hyaluronidases @ 24 h (centre right) and HLC-treatment + chondABC (far right) for 24 h (except for the condition *HLC-treatment + hyaluronidases @ 24 h* (HLC-treatment for 48 h with addition of hyals at 24 h)).

(B) Quantification of the CP/VZ ratio of HA immunoreactivity in 12-14 GW huNcx in FFTC subjected to control and HLC-treatment + chondABC for 24 h. *, $P=0.0201$.

(C) DAPI staining (blue) and IF for HA (red) in the CP of 22 GW huNcx in FFTC subjected to control (left) and treatment with HAS inhibitor (right) for 4 days.

(D) Quantification of GI in 22 GW huNcx in FFTC subjected to the indicated treatments for 24 h. *, $P=0.0379$.

(E) Quantification of gyrus CP thickness (filled triangles, left y-axis) and intergyral distance (open circles, right y-axis) relative to sulcus CP thickness, in 11-16 GW neocortex in FFTC for 24 h subjected to HLC-treatment and 22 GW neocortex in FFTC for subjected to HLC-treatment or control for 4 days. Blue dashed line delineates sulcus CP thickness, set to 1.0.

(F) Quantification of the CP/VZ ratio of HA immunoreactivity in 22 GW huNcx in FFTC subjected to control and treatment with HAS inhibitor for 4 days. **, $P=0.0087$.

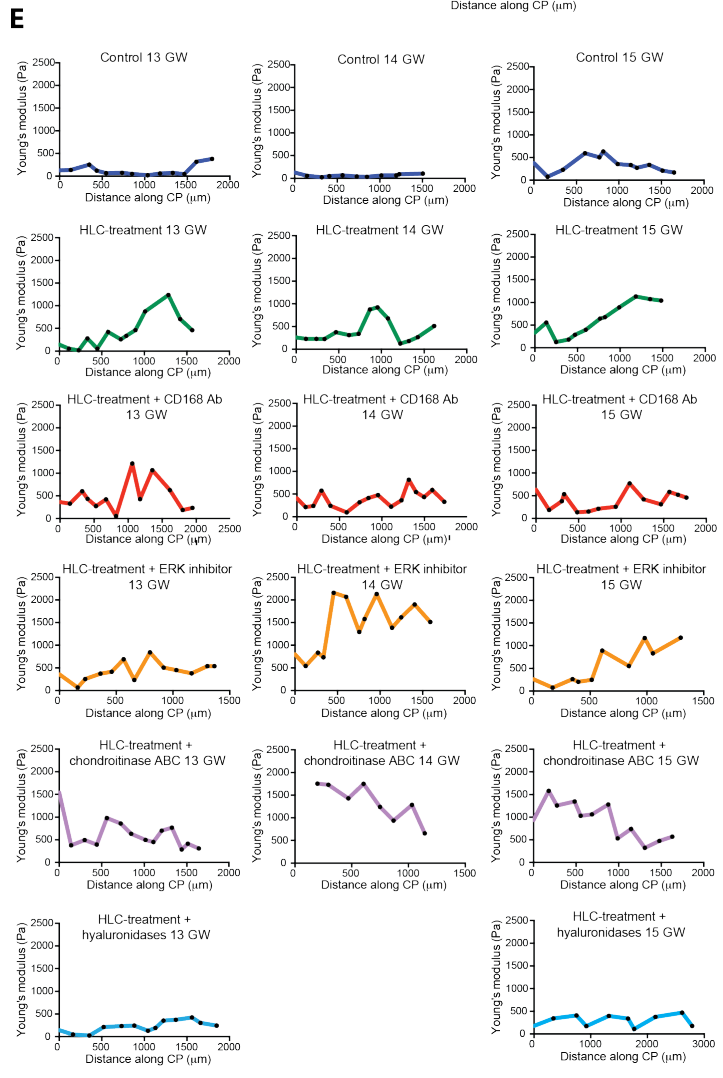
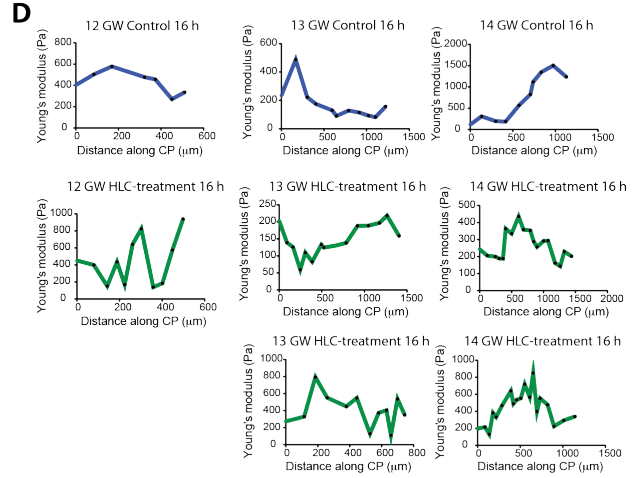
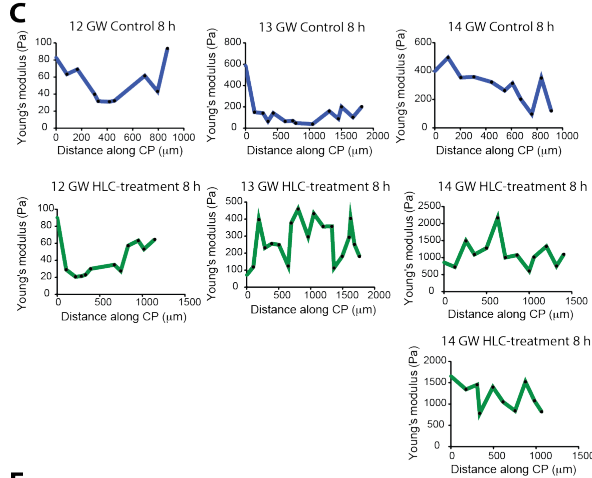
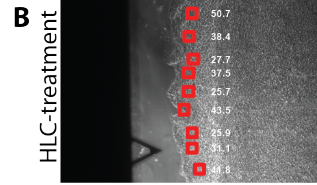
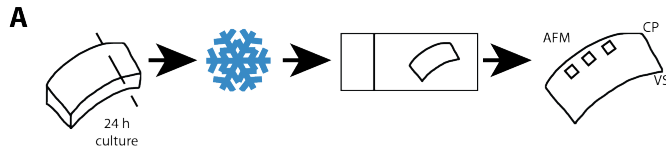
(G) Quantification of GI of 22 GW huNcx in FFTC subjected to the indicated treatments for 24 h. *, $P=0.0247$ (control vs. hyals), $P=0.0394$ (control vs. HAS inhibitor).

(H-M) Quantification of the average distance between nuclei (H, J, L) in the gyri vs. sulci in the CP of non-cultured 22 GW neocortex **, $P=0.0068$ (H, I), in the CP of 11-14 GW neocortex in FFTC subjected to control and HLC-treatment for 8 h (J, K) and 16 h (L, M, separate analysis of HLC-induced gyri vs. sulci) was determined, *, $P=0.0452$. (I, K, M) Frequency distribution histograms for the distance between nuclei. Note the shift to the right upon HLC-treatment already after 8 h (I), and in HLC-induced (K) and physiologically formed (M) gyri vs. sulci.

(N) Quantification of p90RSK immunoreactivity in the CP of 13-16 GW huNcx in FFTC subjected to the indicated treatments for 24 h, relative to control indicated by the blue dashed line (set to 1.0). *, $P=0.363$.

(**O**) DAPI staining (blue) and p90RSK IF (grey) in the CP of 14 GW huNcx in FFTC subjected to control (top), HLC-treatment (middle) and HLC-treatment + ERK inhibitor (bottom) for 24 h. (**E, F, O**) Scale bars: (**E, F**) 200 μm and (**O**) 50 μm .

(**A-E, F-K**) Statistical tests used; one-way ANOVA (**A, E, J**), Student's *t*-test (**B, D, F, H**). Error bars, SD; ns, $P > 0.05$. (**A-E**) Data points represent 3 ind. exp. (1 fetus/exp.) with 1-2 FFTCs per condition per fetus. (**F, H, J**) Data are presented as whisker plots showing the minimum, mean and maximum values. Error bars, SEM; ns, $P > 0.05$; *, $P < 0.05$; **, $P < 0.01$. (**F-K**) The data in each graph represent 3 ind. exp. (1 fetus/exp.) with 1-2 FFTCs per condition.



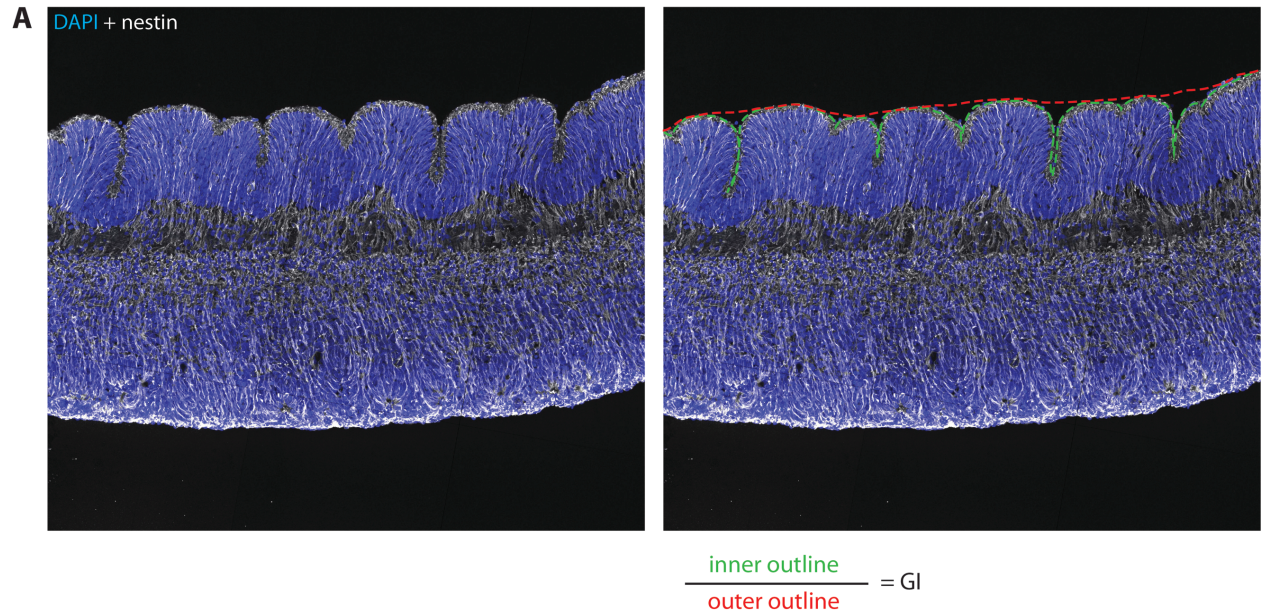
Supplemental Figure 8. AFM measurements of HLC-induced ECM stiffness changes at the onset of HLC-induced folding in 12-14 GW huNcx and in 13-15 GW huNcx after various treatments at 24 h in FFTC. Related to Figure 5.

(A) Schematic of the steps performed to prepare human fetal (and embryonic ferret) neocortex for AFM measurements; (i) FFTC followed by preparation of tissue slices; (ii) freeze-thawing of tissue slices; (iii) cryosectioning of tissue slices followed by thawing and drying; (iv) AFM measurements of CP ECM stiffness on these cryosections. VS, ventricular surface.

(B) Bright-field image of a cryosection of 13 GW huNcx after HLC-treatment in FFTC for 24 h, prepared for AFM measurement. Red boxes delineate the areas measured; within each box 9 measurements were taken. Numbers indicate the average Young's modulus value for each box measured.

(C, D) AFM measurements in the CP of 12 (top rows), 13 (middle rows) and 14 (bottom rows) GW huNcx in FFTC subjected to either control (blue) or HLC-treatment (green) for 8 h (C) and 16 h (D), plotted against the distance measured along the length of the CP from the first point measured (0) (in μm). Each graph represents one FFTC from one fetus.

(E) AFM measurements in the CP of 13 (left column), 14 (middle column) and 15 (right column) GW huNcx in FFTC subjected to either control (dark blue), HLC-treatment (green), HLC-treatment + CD168 antibody (red), HLC-treatment + ERK inhibitor (orange), HLC + chondABC (purple) and HLC-treatment + hyals (light blue) for 24 h, plotted against the distance measured along the length of the CP from the first point measured (0) (in μm). Each graph represents one FFTC from one fetus.



Supplemental Figure 9. Method of GI measurement. Related to Figure 2.

(A) DAPI staining (blue) and nestin immunofluorescence (grey) of 13 GW huNcx after HLC-treatment. Image on the right shows how GI was measured: the inner, folded outline of the basal side of the CP (dashed green line) is divided by the hypothetical, smooth outline of the basal side of the CP (dashed red line).

Table S2. List of primers used for mRNA level analysis by qPCR. Related to STAR methods.

Gene symbol	forward primer	reverse primer
<i>HAS1</i>	GTAGCCTTCAATGTGGAGCG	CAGGCCTCAAGAAACTGCTG
<i>HAS2</i>	GGACGACTTTATGACCAAGAGC	GCAGCTGTGATTCCAAGGAG
<i>HAS3</i>	GCGATTCGGTGGACTACATC	TCCAGGACTCGAAGCATCTC
<i>HYAL1</i>	TCTGGGTGAGCTGGGAAAAT	GAAGGGCCCCAGTGTAGTG
<i>HYAL2</i>	GTCTTCACACGACCCACCTA	GCACTCTCGCCAATGGTAGA
<i>HYAL3</i>	CCTATGTCCGCCTCACACA	CTGCACTCACACCAATGGAC
<i>HYAL4</i>	GCAGGCATTGTTATTTGGGGA	AGCTCTGGTCACATTGGCTA
<i>HPRT1</i>	GCTGAGGATTTGGAAAGGGTG	GCTACAATGTGATGGCCTCC